치의과학박사 학위논문

Effects of CPNE7 on Odontoblasts and Hepatocytes Based on Mitochondrial Function

미토콘드리아 기능에 기반하여 CPNE7이

상아모세포 및 간세포에 미치는 영향

2023년 2월

서울대학교 대학원

치의과학과 세포 및 발생생물학 전공

황 금 빛

Effects of CPNE7 on Odontoblasts and Hepatocytes Based on Mitochondrial Function

지도 교수 박 주 철

이 논문을 치의과학박사 학위논문으로 제출함
2022년 11월

서울대학교 대학원
치의과학과 세포 및 발생생물학 전공
황 금 빛

황금빛의 치의과학박사 학위논문을 인준함
2023년 01월

위 원 장 _____ 한 승 현 _____ (인)

부위원장 _____ 박 주 철 _____ (인)

위   원 _____ 김 홍 중 _____ (인)

위   원 _____ 김 진 만 _____ (인)

위   원 _____ 김 성 진 _____ (인)

Effects of CPNE7 on Odontoblasts and Hepatocytes Based on Mitochondrial Function

Directed by Prof. Joo−Cheol Park, D.D.S., PH.D.

Submitting a Ph.D. Dissertation of Dentistry

November 2022

Graduate School of Dentistry
Seoul National University
Cell and Developmental Biology Major

Geumbit Hwang

Confirming the Ph.D. Dissertation written by
Geumbit Hwang
January 2023

Chair	<u>Seung Hyun Han</u>	(Seal)
Vice Chair	<u>Joo−Cheol Park</u>	(Seal)
Examiner	<u>Heung Joong Kim</u>	(Seal)
Examiner	<u>Jin Man Kim</u>	(Seal)
Examiner	<u>Sung−Jin Kim</u>	(Seal)

Abstract

Effects of CPNE7 on Odontoblasts and Hepatocytes Based on Mitochondrial Function

Geumbit Hwang

Program in Cell and Developmental Biology

Department of Dental Science

Graduate School

Seoul National University

Directed by Prof. Joo−Cheol Park, D.D.S., Ph.D.

Copine7 (CPNE7) belongs to the ubiquitous copine family of calcium−dependent phospholipid binding proteins. During tooth development, CPNE7, a dental epithelium−derived factor, is expressed in preameloblasts, secreted extracellularly, and translocated to preodontoblast to regulate odontoblast differentiation. Recently, it has been reported that CPNE7 plays an important role in physiological dentin regeneration by reactivating the function of mature odontoblasts via autophagy induction. To determine the biological role of CPNE7, $Cpne7$−null ($Cpne7^{-/-}$) mice were generated by deleting Exons 5, 6, and 7 of the $Cpne7$ gene through the gene targeting system. In histological analysis of $Cpne7^{-/-}$ mice, formation of impaired odontoblast and aberrant

i

dentin were observed. Besides the mechanisms involved in autophagy induction, CPNE7 is also involved in calcium flux due to its high calcium ion binding affinity. Furthermore, reactive oxygen species (ROS), which lead to oxidative stress, can be removed by CPNE7. Both calcium flux and ROS are intimately linked to mitochondrial function. In addition, it is known that odontoblast differentiation and dentin formation are affected by mitochondrial function. However, it is unclear whether mitochondria are involved in the physiological dentin formation by mature odontoblasts.

In histological analysis of $Cpne7^{-/-}$ mice, hepatic lipid accumulation was also observed. A recent study reported that abnormalities in fatty acid and lipid metabolism were linked to the gene variant of CPNE7. Hepatic lipid is produced by the influx of fatty acids through de novo lipogenesis, adipose tissue lipolysis, and reabsorption in circulation. The beta-oxidation of fatty acids in mitochondria removes hepatic lipids. Mitochondrial dysfunction affects hepatic lipid homeostasis and promotes reactive oxygen species (ROS) generation. However, studies on CPNE7 in the liver and hepatic mitochondria have not yet been conducted.

Therefore, the purpose of this study is to examine how CPNE7 has an impact on mitochondria of odontoblasts and hepatocytes. The measurement of mitochondrial respiration was performed in hDPCs under oxidative stress followed by CPNE7-derived oligopeptide (CPNE7-DP) treatment. CPNE7-DP treatment in H_2O_2-treated hDPCs significantly increased maximal mitochondrial respiration. Histological analysis and microleakage test were conducted after

brushing experiments with the toothpastes containing CPNE7-DP and other active desensitizing ingredients in a hypersensitivity model *in vitro* and *in vivo*. Among the *in vivo* dentin hypersensitivity models, the formation of tertiary dentin was observed in the experimental group with CPNE7-DP-containing toothpaste, whereas no new hard tissue formation was observed in experimental group with commercially available desensitizing toothpastes. Microleakage analysis revealed that CPNE7-DP-containing toothpaste induced significantly lower dental fluid flow than control.

To investigate the function of CPNE7 in hepatocytes, a non-alcoholic fatty liver disease (NAFLD) model was prepared by feeding a high-fat diet (HFD) in *Cpne7*$^{-/-}$ mice and *Cpne7*-overexpressing transgenic (*Cpne7* Tg) mice. In these models, histological analysis, western blot, measurement of ROS level, and the analysis of mitochondrial function were conducted. *Cpne7* deficiency promoted severe hepatic steatosis in the HFD-induced NAFLD model. More importantly, mitochondrial dysfunction was observed along with an imbalance of mitochondrial dynamics in the livers of HFD-fed *Cpne7*$^{-/-}$ mice, resulting in high ROS levels. Consistent with *in vivo* findings, high ROS levels, mitochondrial dysfunction and lipid accumulation were observed *in vitro* H_2O_2-treated shCPNE7 HepG2 cells.

Therefore, this study suggests the possibility that CPNE7-DP can enhance mitochondrial function of odontoblasts, leading to tertiary dentin formation and dentin sealing effect under oxidative

stress. In the liver, *Cpne7* deficiency causes excessive ROS formation and mitochondrial dysfunction, which aggravates lipid metabolism abnormalities. Altogether, CPNE7 affects the mitochondrial function of both odontoblasts and hepatocytes.

Table of Contents

List of Figures and Tables

Abbreviations

ALT	Alanine aminotransferase
CD	Chow diet
Cpne7	Copine7
Cpne7$^{-/-}$	Cpne7-null
CPNE7-DP	CPNE7-derived oligopeptide
Cpne7 Tg	Cpne7-overexpressing transgenic
DCFDA	2, 7-dichlorofluorescin diacetate
DEG	Differentially expressed gene
DRP1	Dynamin-related protein 1
DXA	Dual-energy x-ray absorptiometry
EDTA	Ethylenediaminetetraacetic acid
FC	Fold change
FFA	Free fatty acid
FIS1	Mitochondrial fission protein 1
GO	Gene ontology
H&E	Hematoxylin and eosin
HFD	High-fat diet
K14	Keratin-14
LD	Lipid droplet
MFF	Mitochondrial fission factor
MFN1	Mitofusin 1
MFN2	Mitofusin 2

NAFLD	Non-alcoholic fatty liver disease
NASH	Non-alcoholic steatohepatitis
PBS	Phosphate-buffered saline
ROS	Reactive oxygen species
SEM	Scanning electron microscopy
T.col	Total cholesterol
TEM	Transmission electron microscopy
TG	Triglyceride
WT	Wild-type

Chapter I. General introduction

1. Copines

Copines (CPNE) are a highly conserved Ca^{2+}-dependent phospholipid-binding protein family that has two C2 domains (C2A and C2B) and one von willebrand factor A domain (Creutz et al. 1998). The C2 domain is involved in Ca^{2+}-dependent phospholipid binding, and the von Willebrand factor A domain is known to mediate protein-protein interactions by binding to the tetratricopeptide repeat domain(Nalefski and Falke 1996). Copines are almost found in eukaryotes (although they are absent from yeast and Drosophila). Copines typically exist in a family of multiple homologs in a given organism, with humans having 9 copines, nematodes having 6, Dictyostelium having 6, and plants having at least 3. This copine family's high degree of conservation and diversity strongly implies that copines perform fundamentally significant roles in cell biology (Creutz 2012).

Schematic diagram of the common domain structure of copines. Copines has two C2 domains in the N-terminal region and a von Willebrand factor A (vWA) domain in the C-terminal region.

2. Copine 7(CPNE7)

One copine, copine 7(CPNE7) is expressed in brain, testis, and small intestine (Savino et al. 1999). During tooth development, CPNE7, a dental epithelium-derived factor, is expressed in preameloblasts, secreted extracellularly, and translocated to preodontoblast to regulate odontoblast differentiation (Oh et al. 2015; Seo et al. 2017). Recently, CPNE7 reactivates mature odontoblasts and promotes the formation of physiological dentin (Park et al. 2021). To use the CPNE7 protein more reliably, affordably, and effectively, functional peptide was created to mimic its function. CPNE7-derived oligopeptide (CPNE7-DP) is a synthetic peptide covering the linker region of hCPNE7 (344-353 fragment). The amino acid sequence of CPNE7-DP was "Lys-Tyr-Lys-Gln-Lys-Arg-Arg-Ser-Tyr-Lys". CPNE7-DP induces odontoblast differentiation and promotes the regeneration of physiological dentin similar to CPNE7 (Lee et al. 2020).

CPNE7-DP

STTFEEMQKAFEEGQAQWDCVNP**KYKQKRRSYK**NSGVVVLADLKFHRVYSFLDYIMGGCQIHFTVAIDFTASNGDPRNSCSLHYINPYQP

| End of C2B domain | Linker region | Start of vWA domain |
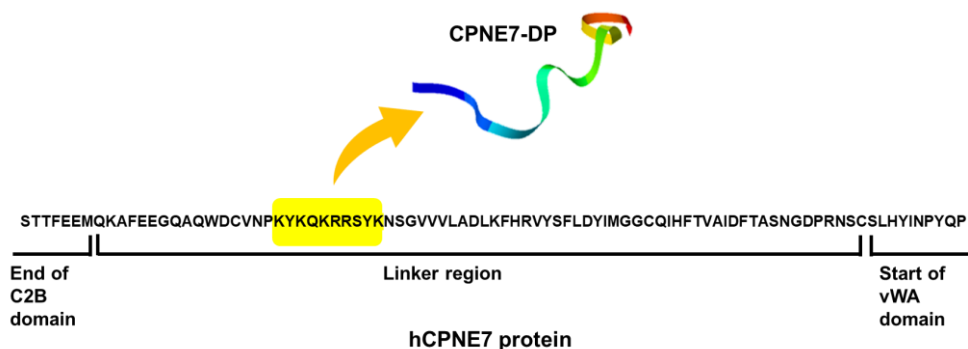
hCPNE7 protein

Schematic illustration of CPNE7-derived oligopeptide (CPNE7-DP) synthesis. CPNE7-DP was derived from the conserved amino acid sequence of the linker region of the hCPNE7 protein.

3. *Cpne7*-null (*Cpne7$^{-/-}$*) mice

To determine the biological role of CPNE7, *Cpne7*-null (*Cpne7$^{-/-}$*) mice were generated by deleting Exons 5, 6, and 7 of the *Cpne7* gene through the gene targeting system and cloning a vector containing EGFR and NeoR. *Cpne7$^{-/-}$* mice were identified by PCR. The primers used were exon 7 F (5'-CAGAAGGCCTTTGAGGAGGAGC-3', deleted region), neo F (5'-CAA TATGGGATCGGCCATTGAAC -3', *Cpne7$^{-/-}$* vector sequence) and exon 8 RR (5'-GTTTGTACTTGGCAT TCACACAGTCC-3').

In histological analysis of *Cpne7$^{-/-}$* mice, abnormalities of dentin and liver were observed (unpublished data). In the dentin-pulp complex of *Cpne7$^{-/-}$* mice, impaired odontoblast and formation of aberrant dentin were observed. Additionally, numerous lipid droplets were accumulated in the liver of *Cpne7$^{-/-}$* mice. Dentin is formed by odontoblasts, and the liver is composed mainly of hepatocytes. Therefore, deeper studies on the role of *Cpne7* in odontoblasts and hepatocytes are required.
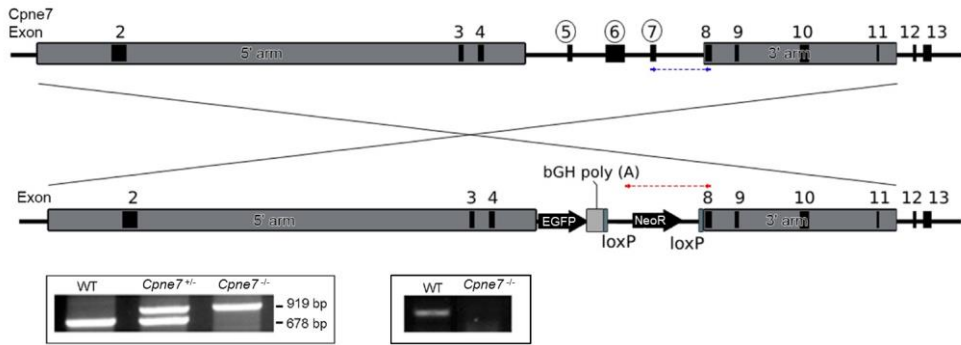
Schematic diagram of generation of *Cpne7*-null (*Cpne7*^−/−^) mice. *Cpne7*^−/−^ mice were generated by deleting Exons 5, 6, and 7 of the *Cpne7* gene through the gene targeting system and cloning a vector containing EGFR and NeoR. *Cpne7*^−/−^ mice were verified by PCR.

4. Roles and mechanisms of action of CPNE7 in odontoblast reactivation and homeostasis

Previous studies have shown that CPNE7 binds to the cell surface receptor, nucleolin to induce autophagy, which in turn activates mature odontoblasts by upregulating DSP, DMP1, Nestin, and Tau (Park et al. 2021; Seo et al. 2017). In addition to mechanism related to autophagy induction, CPNE7 is involved in calcium flux due to its high calcium ion−binding affinity (Choung et al. 2016). Furthermore, CPNE7 has the ability to scavenge reactive oxygen species (ROS) that cause oxidative stress (unpublished data). Calcium flux and ROS are both closely related to the function

of mitochondria, the powerhouse of the cell (Brookes et al. 2004). In addition, it is known that mitochondrial function affects odontoblast differentiation and dentin formation (Imhof et al. 2020). Therefore, further studies are needed to investigate whether CPNE7 is involved in mitochondrial function, resulting in odontoblast reactivation and homeostasis.

5. Predicted mechanism of action of CPNE7 in hepatic lipogenesis

Since lipid accumulation was observed in the liver of $Cpne7^{-/-}$ mice, a preliminary study was conducted to investigate how $Cpne7$ is involved in lipid metabolism. Considering that impaired autophagy can contribute to lipid accumulation, we examined whether $Cpne7$ has a role in inducing autophagy in hepatocytes as it does in odontoblasts. However, there was no difference in autophagy markers between liver tissues of WT and $Cpne7^{-/-}$ mice. Additionally, HepG2 cells, a hepatocyte cell line, were treated with rCPNE7, but no change in autophagy markers was confirmed (data not shown). On the other hand, lipid droplets and mitochondrial morphological abnormalities were observed in the histological analysis of the livers of $Cpne7^{-/-}$ mice using TEM. These findings imply that lipid accumulation in the livers of $Cpne7^{-/-}$ mice is connected to mitochondrial dysfunction.

6. Rationale and outline of the thesis experiments

Altogether, CPNE7 is expected to play a role in mitochondrial function in odontoblasts and hepatocytes. Therefore, a key purpose of this thesis is to investigate 1-1) whether CPNE7-DP affects the mitochondrial function of odontoblast under oxidative stress, 1-2) the effect of toothpastes containing CPNE7-DP in the dentinal microleakage, tubule occlusion and tertiary dentin formation, and 2) the role of *Cpne7* in hepatic fat accumulation based on mitochondrial function. To examine these objectives, the mitochondrial function was measured following CPNE7-DP treatment in ROS-damaged human dental pulp cells (hDPCs). In addition, experimental groups including CPNE-DP-containing toothpastes were investigated by histological and microleakage analysis *in vitro* and *in vivo* hypersensitivity models. In hepatocytes, a non-alcoholic fatty liver disease (NAFLD) model was induced by high-fat diet (HFD) in *Cpne7*$^{-/-}$ mice and *Cpne7*-overexpressing transgenic (*Cpne7* Tg) mice. Macroscopic analyses, dual-energy x-ray absorptiometry (DXA), histological analysis, measurement of ROS levels, assay of mitochondrial function, and western blot were performed. These results confirmed *in vitro* experiments using H_2O_2-induced *CPNE7*-silenced and -overexpressed HepG2 cells.

Chapter Ⅱ.

Research projects

Part 1.

Desensitizing toothpastes

for dentin sealing and tertiary dentin formation

in vitro and in vivo: a comparative analysis

1. Introduction

1.1 ROS in the oral cavity

The oral cavity is the only area of the human body that is exposed to a wide range of external stimuli, including food, air, bacteria, viruses, and fungi, and xenobiotics. Some of these substances have been shown to have considerable oxidizing potential and the capacity to produce reactive oxygen species (ROS) (Zukowski et al. 2018). ROS are a class of unstable and highly reactive molecules, generally produced as a by-product of cellular processes involving molecular oxygen. A moderate level of ROS is beneficial for various physiological processes including antimicrobial activity. However, excessive ROS can damage cellular proteins, lipid, or DNA, impairing normal cellular functions (Plumlee and Ziegler 2007; Wang and Zou 2018). ROS include superoxide anion ($O_2 \cdot ^-$), hydrogen peroxide (H_2O_2), hydroxyl radical($\cdot OH$) (Zukowski et al. 2018). Excessive ROS cause oxidative stress, which could damage several tissues and cells in the oral cavity. Oxidative stress is considered as one of the pathogenesis factors of oral diseases, including periodontitis, xerostomia, and oral cancer (Kumar et al. 2017; Zukowski et al. 2018).

1.2 Interactions between ROS, mitochondria, and tooth homeostasis

Mitochondria are the main source of ROS, and conversely, have an antioxidant system that play a role in scavenging ROS.

Mitochondria are dual membrane-bound organelles that produce most of the chemical energy in the form of adenosine triphosphate (ATP) (Ernster and Schatz 1981; Tielens et al. 2002). Electron transfer during mitochondrial respiration leads to the production of radicals and other reactive oxygen species, generally represented as ROS (Brand et al. 2004; Venditti et al. 2013). These ROS can be eliminated by enzymatic antioxidants such as catalase, superoxide dismutase (SOD) and glutathione peroxidase (GPx)(Chih-Hung and Pei-Chung 2012). Therefore, mitochondria are crucial for ROS homeostasis. Furthermore, mitochondrial dysfunction leads to excessive ROS formation and overproduction of ROS also cause mitochondrial dysfunction (Guo et al. 2013; Murphy 2013).

Mitochondria are involved in tooth development and homeostasis. Tooth development is initiated by a series of reciprocal interactions between ectodermal tissue and the underlying mesenchymal tissue, resulting in the differentiation of ameloblasts and odontoblasts (Cobourne and Sharpe 2003). Ameloblasts and odontoblasts differentiate from oral ectodermal cells and ectomesenchymal cells of dental papilla, respectively (Ruch et al. 1995; Zeichner-David et al. 1995). The functional differentiation of ameloblasts and odontoblasts is significantly influenced by mitochondria. The secretory and maturation stage of enamel differ in mitochondrial morphology and function(Costiniti et al. 2020). The integrity of ameloblasts depend on mitochondrial generated ROS (Eckstein et al. 2019; Eckstein et al. 2017). Furthermore, odontoblast differentiation and dentin formation were

1 0

promoted by mitochondrial fusion in response to DRP1 inhibition (Matsuishi et al. 2018). Recent study reported that mitochondrial function is crucial for Ca2+ homeostasis to synthesize amelogenin, to form enamel matrix, and to induce dental papilla cells to differentiate into odontoblasts (Imhof et al. 2020). In addition, since odontoblast is a post-mitotic cell, as aging progresses, dentin-secretory activity decreases and ROS accumulates (Couve et al. 2013). However, it is unknown whether mitochondria are involved in the physiological dentin formation by mature odontoblasts.

1.3 Dentin hypersensitivity and desensitizing toothpastes

Dentin hypersensitivity is a prevalent problem in dental practice and affects approximately 25% of the adult population (Favaro Zeola et al. 2019; Splieth and Tachou 2013). It is described as brief but sharp pain that arises from exposed dentin in response to external stimuli and that cannot be attributed to any other form of dental disease or defect (Holland et al. 1997). Among the explanations for these painful response, the hydrodynamic theory is generally accepted (Pashley and Galloway 1985). According to this theory, the cause of dentin hypersensitivity is the increased fluid movement within open dentinal tubules (Brannstrom 1986). The painful symptoms of dentin hypersensitivity can be reduced by dentinal tubule occlusion (Brannstrom 1986; Pashley 1986).

Desensitizing toothpaste—a dental product used at home—is the first choice for dentin hypersensitivity owing to its convenience, low cost, and noninvasiveness (Arnold et al. 2016; Cunha-Cruz et

al. 2010). Various desensitizing toothpastes are commercially available. These toothpastes exert their effect by blocking pulpal nerve responses or occluding dentinal tubules (Addy and West 2013). Toothpastes for blocking pulpal nerve response contain potassium salts; however, the efficacy of potassium salts is controversial (Addy and West 2013; Sharma et al. 2012). The majority of desensitizing toothpastes work by occluding dentinal tubules and contain several active ingredients, including calcium carbonate, arginine, and strontium acetate (Addy and West 2013; Miglani et al. 2010). Previous studies have demonstrated that these active ingredients act as desensitizing agents by reducing pain (Docimo et al. 2009; Fu et al. 2010; Gedalia et al. 1978; Pearce et al. 1994; Silverman et al. 1996). Although tubule occlusion was observed in several studies, it was superficial and not resistant to acid challenges and saliva immersion (Arnold et al. 2015; Gandolfi et al. 2008). Therefore, desensitizing agents with long-term tubule-occluding effects must be developed using appropriate assessment methods.

1.4 Copine 7 (CPNE7)

The copine family comprises ubiquitous calcium-dependent, phospholipid-binding proteins that are highly conserved across several species (Tomsig and Creutz 2002). One copine, CPNE7, reactivates odontoblasts and promotes the formation of physiological dentin (Park et al. 2021) and reacts with calcium ion in dentinal fluid owing to its high calcium ion-binding affinity

(Choung et al. 2016). In a dentin hypersensitivity model, CPNE7 induced biological dentin sealing, and the effect was permanent rather than transient (Park et al. 2019). Subsequently, Lee et al. synthesized CPNE7-derived oligopeptide (CPNE7-DP), which, as recombinant CPNE7 protein, also induced dentinal tubule occlusion (Lee et al. 2020).
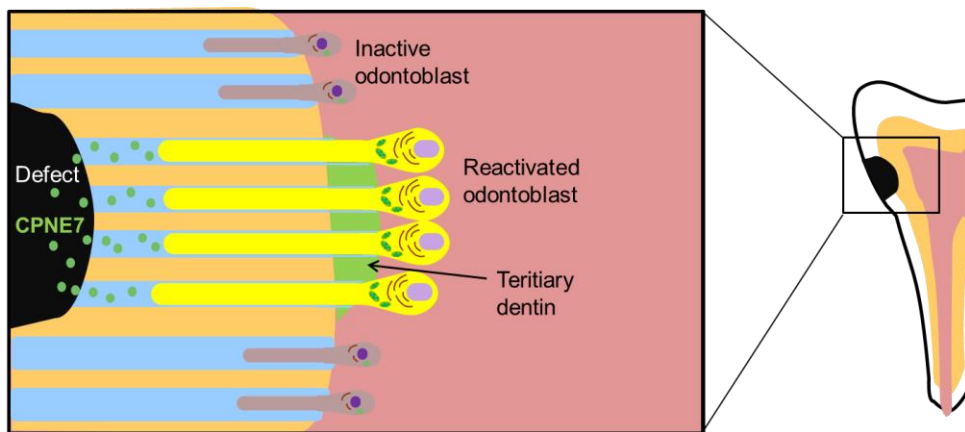
Schematic depiction of odontoblast reactivation by CPNE7.
CPNE7 reactivates mature odontoblasts and promotes tertiary dentin formation.

1.5 Purpose of research

Therefore, this study aimed to evaluate 1) whether CPNE7-DP affects the mitochondrial function of odontoblast under oxidative stress, and 2) the effect of toothpastes containing CPNE7-DP in the dentin sealing and tertiary dentin formation

2. Materials and Methods

2.1. Human dentin preparation

The experimental protocol for this study was approved by the Institutional Review Board in Seoul National University Dental Hospital, Seoul, Korea (S-D20140007). The experiments involving extracted human teeth were performed in accordance with the Declaration of Helsinki. Informed written consent was obtained from each participant prior to the experiments. Five extracted human molars were obtained from Seoul National University Dental Hospital, stored in phosphate-buffered saline (PBS) at 4° C before use, and then sectioned mid-coronally into 1-mm-thick dentin disks. Each disk was sectioned into four fan-shaped pieces by a low-speed diamond wheel saw (Model 650; South Bay Technology Inc., San Clemente, CA, USA) under constant water cooling. The pieces were rinsed with PBS twice for 5 min each and immersed in 0.5-M ethylenediaminetetraacetic acid (EDTA) solution for 5 min to remove inorganic debris. The processed pieces were then washed again with PBS twice for 5 min each. To remove the smear layer and fully open the dentinal tubules, the pieces were etched with 32% phosphoric acid for 5 min and sonicated by an ultrasonic processor (VCX-750; Sonics & Materials, Inc., Newtown, CT, USA) six times for 5 min each. The pieces were washed with 1X PBS three times for 5 min each and then stored in artificial saliva. The artificial saliva consisted of 0.7-mM $CaCl_2$, 30-mM KCl, 0.2-

1 4

mM MgCl2•6H2O, 4.0-mM NaH2PO4, 0.3-mM NaN3, and 20-mM HEPES buffer(Pashley et al. 2004).

2.2. In *vitro* treatment of human teeth

From the five human teeth, 20 dentin disks were randomly divided into five groups (n=4). The disks in the negative control group were kept in artificial saliva and were not brushed at all. The disks in the other four groups were brushed with different toothpastes: group 1 (control), with toothpaste not containing any desensitizing ingredients; group 2, with toothpaste containing CPNE7-DP (HysensBio Co., Ltd., Gwacheon, Korea); group 3, with Colgate Sensitive Complete Protection Toothpaste (Colgate-Palmolive Company, New York, NY, USA); and group 4, with Sensodyne Rapid Relief (GlaxoSmithKline, Brentford, UK). The toothpastes had different active ingredients, which are summarized in Table 1.

Each group was divided into two subgroups characterized by the duration of toothpaste application (2 weeks or 4 weeks); each subgroup comprised two dentin disks. The toothpastes were applied to the disks with microbrushes (M6500-F Micro Applicator; TPC Advanced Technology Inc., City of Industry, CA, USA), and each disk was manually brushed for 1 min twice a day for 2 or 4 weeks. After each brushing session, the disks were washed with distilled water and immersed in artificial saliva until the next brushing session.

Table 1. Summary of the experimental groups

Group	Product name	Active ingredient	Company
1	Control (non-desensitizing ingredients)	—	
2	CPNE7-DP-containing toothpaste	CPNE7-DP	HysensBio Co.
3	Colgate Sensitive Pro-Relief Complete Protection	Calcium carbonate, arginine	Colgate-Palmolive Company
4	Sensodyne Rapid Relief	Strontium acetate	GlaxoSmithKline

CPNE7-DP: CPNE7-derived peptide

2.3. Preparation of experimental toothpastes

The toothpastes of Group 1 (Control) and Group 2 (CPNE7-DP-containing toothpaste) were manufactured in the lab, excluding the two commercial toothpastes. The toothpaste of Group 2 was the addition of CPNE7-DP to the toothpaste of Group 1, and all other components are the same. CPNE7-DP was synthesized as mentioned in the previous study (Lee et al. 2020). For experimental toothpaste production, first, purified water and D-sorbitol solution were mixed. Second, Tricalcium phosphate, aminocaproic acid, allantoin, hydrous silicic acid, sodium PCA solution, hydroxyapatite,

CPNE7-DP (Group 2 only), enzyme-treated stevia, and xylitol were added and stirred in a stirrer for about 40 minutes. Third, (concentrated) glycerin and xanthan gum were added and stirred for about 40 minutes. Fourth, (concentrated) Glycerin, Carboxymethyl Cellulose Sodium Salt (CMC) were added and stirred for about 40 minutes. Stirring conditions from steps 2 to 4 were as follows; PADDLE 10-30 rpm, DISPERSE 500-600 rpm, HOMO 2400-3200 rpm. Fifth, sodium cocoylmethyltaurate were added and stirred for about 20 minutes. Finally, the Flavoring agents were added and stirred for about 15 minutes. The stirring conditions for steps 5 and 6 were PADDLE 10-30 rpm, DISPERSE 450-650 rpm. Each step is stirred under reduced pressure conditions (-760 mmHg). The detailed ingredients and contents of toothpaste are recorded in Table 2.

Table 2. Ingredient and content of experimental toothpastes

STEP	COMPONENT	INGREDIENT	CONTENT (WT %)
1	Solvent	Purified water	21.587
	Humectant	D-Sorbitol Solution	30
2	Staple	Tricalcium phosphate	32
		Aminocaproic acid	0.2
		Allantoin	2
	Humectant	Sodium PCA solution	3
	Viscosity modifier	Hydrous silicic acid	4

	Diluting agent	Hydryxyapatite	0.05
	Peptide (Group 2 only)	CPNE7-derived oligopeptide	0.002
	Sweetening agent	Enzyme-treated stevia	0.1
		Xylitol	0.1
3	Humectant	(Concentrated) glycerin	2
	Viscosity modifier	Xanthan gum	0.3
4	Humectant	(Concentrated) glycerin	2
	Viscosity modifier	CMC (Carboxymethyl Cellulose Sodium Salt)	0.6
5	Surfactant	Cocoylmethyltaurate	1.2
6	Flavoring agent	Green tea extract	0.01
		Chamomile extract	0.01
		Rosemary extract	0.01
		Myrrh tincture	0.01
		Rhatany tincture	0.01
		Chamomile tincture	0.01
		Mastic oil 40 HF-60662	0.001
		Propolis extract	0.05
		Grapefruit seed extract	0.1
		Spearmint B71228	0.05
		Peppermint oil 81689	0.6
	Total		100

2.4. SEM analysis

The disks brushed with toothpaste were fixed in 0.1 M of cacodylate buffer (pH 7.4) containing 2.5% glutaraldehyde for 30 min and in 0.1 M of cacodylate buffer containing 1% osmium tetroxide for 1 h. The disks were dehydrated in graded acetone and then critical point dried. Each sample was sputter-coated with a thin layer of gold and observed under the scanning electron microscope (S-4700; Hitachi, Ltd., Tokyo, Japan) at an accelerating voltage of 10 kV. For quantification of open dentinal tubules, the void area indicated by open dentinal tubules was analyzed using the particle analysis of Image J

2.5. In *vivo* dentin hypersensitivity model with canine teeth

All experiments involving animals followed the protocols approved by the Ethics and Institutional Animal Care and Use Committee of Seoul National University (SNU-180416-2-1 and SNU-171020-5-2). This study also conformed to the Animal Research: Reporting In Vivo Experiments (ARRIVE) guidelines for preclinical animal studies. Four beagles (aged between 1 and 2 years) were obtained from the Experimental Animal Center of College of Dentistry and Use Committee of Seoul National University and used for the *in vivo* dentin hypersensitivity model. Each group consisted of 1 beagle dog with 10 premolars (2 maxillary premolars and 3 mandibular premolars on each side). Before the preparation of the cervical area on the buccal side, all the calculus was removed. For disinfection before dentin exposure,

the tooth surfaces were swabbed with cotton balls soaked in 0.5% chlorhexidine. To mimic class V cervical lesions in human patients with dentin hypersensitivity, a high-speed handpiece was used to create modified class V-like cavities on the buccal surfaces of the teeth. The depth of the cavities was half the diameter of the high-speed round bur (Carbide Bur FG Round #4, FG4-014; Komet Dental, Lemgo, Germany). The smear layer was removed with 17% EDTA for 2 min. All defects were exposed during the tooth brushing period. All toothpastes were applied using the Bass brushing method, 1.5 min for each quadrant, once daily for 6 weeks. The samples were obtained after vital perfusion with the Karnovsky solution.

2.6. Histological analysis

The premolars (n=5) were extracted, fixed in 4% paraformaldehyde, decalcified in 30% formic acid, and embedded in paraffin. The samples were coronally divided, perpendicular to the cavity, into 5-μm-thick sections. The sections were stained with hematoxylin and eosin and observed under an optical microscope (Axiolab 5; ZEISS Microscopy, Jena, Germany).

2.7. Microleakage analysis

To evaluate the microleakage of dentinal fluid from the cervical lesions, the apical 3 mm of single roots was eliminated (n=5). A high-speed carbide bur (FG#330; SS White Dental, Seoul, Korea) was used to prepare each root end for a 2-mm depth along the root

canal, and a 0.9-mm metal tube was inserted into the canal. To insert the metal tubes, we used 37% phosphoric acid (Any-Etch™; Mediclus Co., Ltd., Cheongju, Korea), adhesive agent (3M™ Single Bond Universal Adhesive; 3M ESPE, St. Paul, MN, USA), and flowable composite resin (3M™ Filtek™ Supreme Ultra Flowable Restorative; 3M, Alexandria, MN, USA). The whole surfaces of the teeth were coated with nail polish several times, except the defect area. The prepared samples were kept in distilled water until the microleakage test. The microleakage test was conducted as previously described (Park et al. 2019): a machine (nanoFlow; IB Systems, Seoul, Korea) was used to measure the movement of the bubbles (indicating leakage) caused by the flow of distilled water from the tooth apex to the exposed dentin at 70-cm H_2O. All measurements were taken at 40 min after connecting the sample. The 20-min outflow was recorded, excluding the initial 20-min outflow.

2.8. Measurement of mitochondrial function

Oxygen consumption rate (OCR) was measured by Seahorse XFe96 Extracellular Flux Analyzer with XF Cell Mito Stress Test Kit as per manufacturer's protocol (Seahorse Bioscience, North Billerica, MA, USA). Briefly, human dental pulp cells(hDPCs) were treated CPNE7-DP (50 μg/ml, 48h) following treatment of H_2O_2 (1 mM, 1h) and were seeded at a density of 2 x 10^4 cells/well onto 96-well cell culture plate for overnight. The medium was replaced the following day to XF running medium with 1 mM sodium pyruvate,

2 mM L-glutamine and 1000 mg/L D-glucose for OCR measurement. Cells were sequentially exposed to Oligomycin (1.5 μM; ATPase inhibitor), FCCP (0.5 μM; mitochondrial uncoupler) and Rotenenone/Antimycin A (0.5 μM; complex I/III inhibitor). The average measurement from experiments conducted in triplicate is shown by each point in the traces.

2.9. Statistical analysis

Statistical analyses were performed using GraphPad Prism software (version 5, GraphPad Software, CA, USA). All values are expressed as the mean ± standard deviation for at least three independent experiments. The normal distribution was confirmed using the Kolmogorov-Smirnov test with Dallal-Wilkinson-Lillie for p-value (alpha=0.05). Between-group statistical analyses were performed using the one-way analysis of variance followed by Tukey's multiple comparison test (p-value < 0.05). Statistically significant differences between groups were considered at *p < 0.05, **p < 0.01 and ***p < 0.001.

3. Results

3.1. Comparison of mitochondrial function

To measure the mitochondrial function—enhancing effect of CPNE7—DP in hDPCs under oxidative stress, hDPCs were exposed to H_2O_2 followed by CPNE7—DP treatment and mitochondrial respiration was measured. As presented in Figure 1, mitochondrial respiration, including basal respiration, ATP production and maximal respiration, was decreased by H_2O_2—induced oxidative stress. CPNE7—DP treatment in H_2O_2—treated hDPCs significantly increased maximal mitochondrial respiration compared to control, CPNE7—DP and H_2O_2—only treated hDPCs. These findings indicate that CPNE7—DP increase mitochondrial function in hDPCs with oxidative stress.

Mitochondrial Respiration
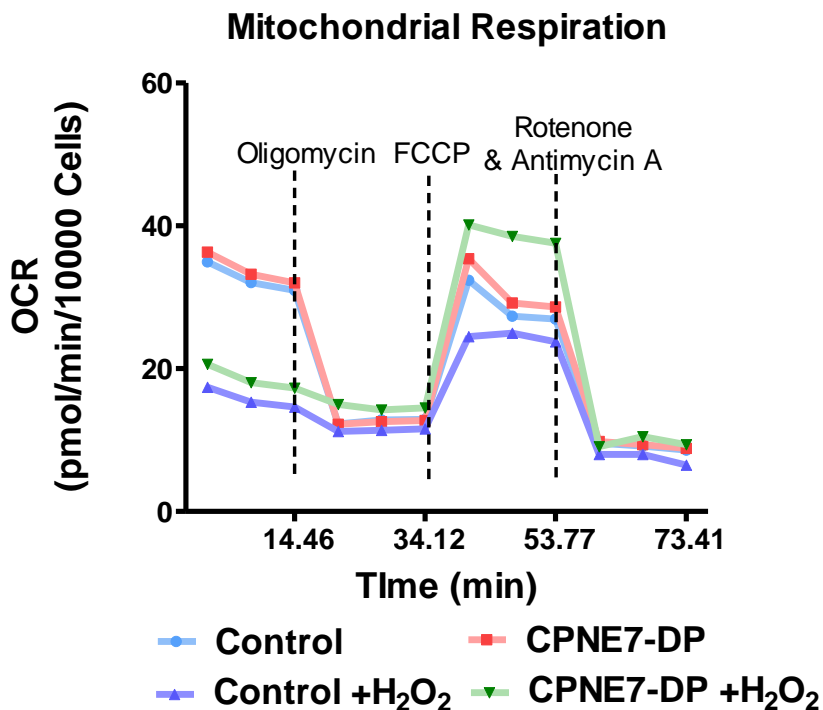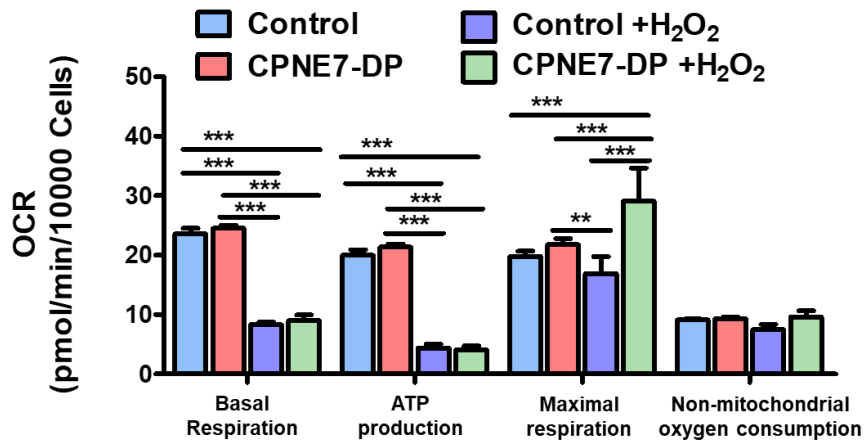
Figure 1. Representative (upper) and statistical results (bottom) of mitochondrial respiration in control and CPNE7−DP treated hDPCs without/with H₂O₂−induced oxidative stress. The mitochondrial respiration was significantly decreased by H_2O_2 treatment (1 mM, 1h). Maximal mitochondrial respiration in H_2O_2 − treated hDPCs was significantly increased followed by CPNE7−DP treatment (50 μg/ml, 48h). (**p <0.01 and ***p <0.001)

3.2. SEM analysis of dentinal tubule

After the 2- or 4-week brushing protocol, the surface images of the dentin disks were analyzed via SEM at 2500x magnification. The negative control disks showed that the smear layer was removed, and dentinal tubules were fully open (Figure 2A, F); on the contrary, all experimental disks revealed partially occluded dentinal tubules (Figure 2B–E, G–J). In groups 2 and 3, the disks brushed for 2 weeks exhibited more tubule occlusion than did those in groups 1 and 4 (Figure 2C, D). Among all experimental groups, the disks brushed for 4 weeks exhibited a slightly heavier deposition on the intertubular dentin and firm occlusion of the dentinal tubules, in comparison with those brushed for 2 weeks. However, we found few other differences in each group between the disks brushed for 2 weeks and those brushed for 4 weeks (Figure 2K).

In quantification graph of the open dentinal tubule by area, most of the dentinal tubule area of negative control with only fully open dentinal tubules were more than 300 μm^2 (Figure 2L, M). As shown in Figure 2L, fully open dentinal tubules (more than 300 μm^2) were decreased in group 1 compared to group 4, and the open dentinal tubules with an area of 100−300 μm^2 were increased in group 1 compared to groups 2 and 3. The open dentinal tubules with an area of 100−300 μm^2 in group 2 were decreased compared to group 4 (Figure 2L). In the disks brushed for 4 weeks, the fully open dentinal tubules (more than 300 μm^2) were decreased group 2 compared to group 3 (Figure 2M). Overall, the percentage of open

dentinal tubules decreased in all groups compared to the negative control, however there was no significant difference between groups. In the disks brushed for 2 weeks, there were differences between group 1 (control) and experimental groups (groups 2, 3 and 4), but not in the disks brushed for 4 weeks, according to the quantification results of the open dentinal tubule by area. Furthermore, dentinal tubule occlusion was observed in group 1 without any desensitizing agents. These results imply that SEM image analysis *in vitro* hypersensitivity model is inadequate for evaluating dentinal tubule occlusion.

	Negative control	Group 1	Group 2	Group 3	Group 4
2 w	A	B	C	D	E
4 w	F	G	H	I	J

K

Open dentinal tubules (%)

Legend:
- Negative control
- Group 1
- Group 2
- Group 3
- Group 4

L

2w

Y-axis: Open dentinal tubules (%)

Legend:
- 10~100
- 100~300
- 300~ (μm^2)

X-axis: Negative control, Group 1, Group 2, Group 3, Group 4

M

4w

Y-axis: Open dentinal tubules (%)

Legend:
- 10~100
- 100~300
- 300~ (μm^2)

X-axis: Negative control, Group 1, Group 2, Group 3, Group 4
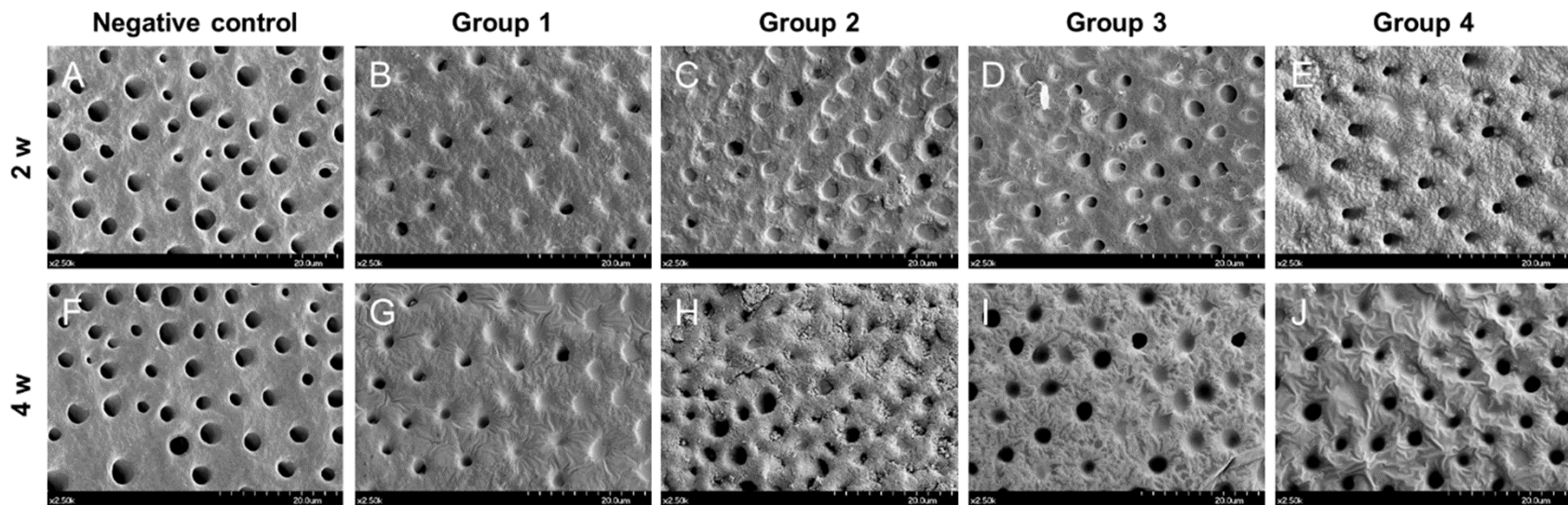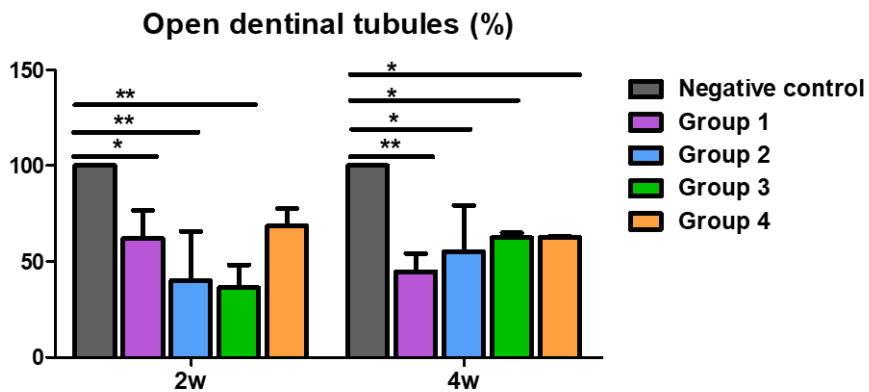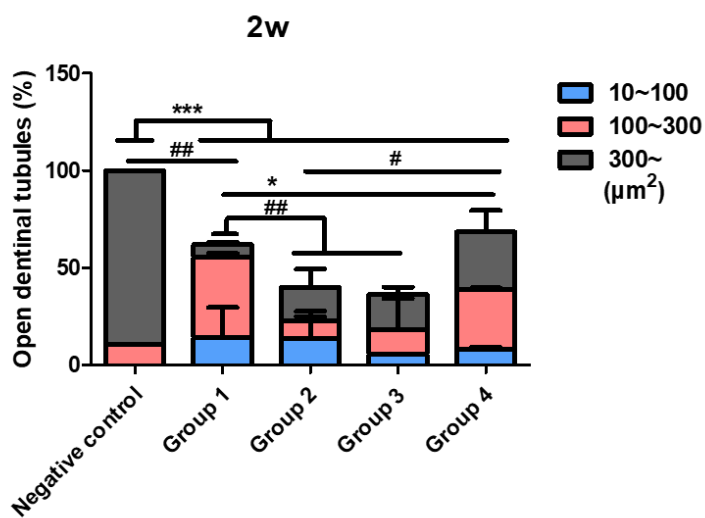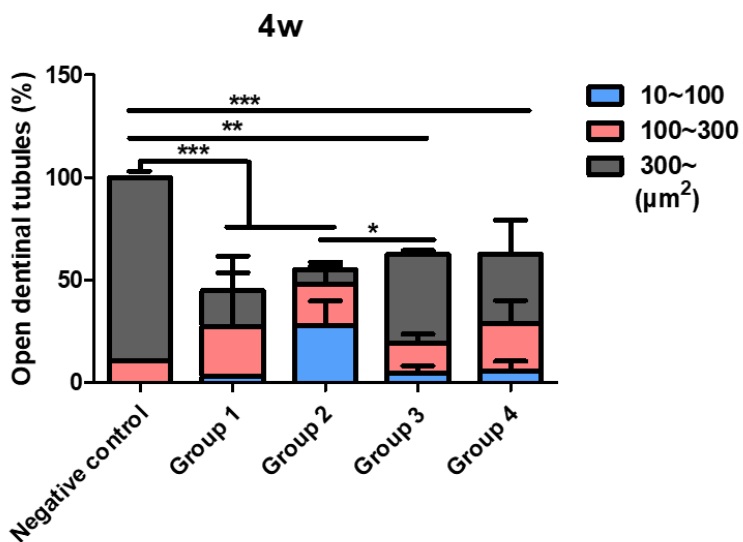
Figure 2. Scanning electron microscopic images of human dentin disks at 2500x magnification, after brushing for 2 or 4 weeks. The upper row presents the disks after 2 weeks of toothpaste application, and the lower row presents those after 4 weeks of application. (A and F) In the negative controls, the dentin surface appeared free of smear layer, and the dentinal tubules were completely open. (B–E and G–J) In the experimental disks, partial occlusion of dentinal tubules was observed. The percentage of open dentinal tubules represented the ratio of the number of open dentinal tubules to the total number of tubules and was classified by area (K−M). ($*p<0.05$, $**p <0.01$ and $***p <0.001$; total open dentinal tubules (%), area with more than 300 μm^2), ($\#$ $p<0.05$, $\#\#$ $p<0.01$; area with $100-300$ μm^2)

3.3. Tertiary dentin formation at the dentin-pulp interface

To evaluate long-term dentin sealing effects, we generated an *in vivo* hypersensitivity model with dogs' teeth. After the exposed dentin area was brushed for 6 weeks, we histologically analyzed the dentin. As presented in Figure 3A, no new mineralized tissue formation was observed in groups 1, 3, and 4. Conversely, group 2 demonstrated newly formed tertiary dentin underneath the tooth defect area; moreover, this newly formed dentin included dentinal tubules (Figure 3B). These findings indicate that only the CPNE7-DP-containing toothpaste caused biological tertiary dentin to form, which could result in a long-term dentin sealing effect.

A
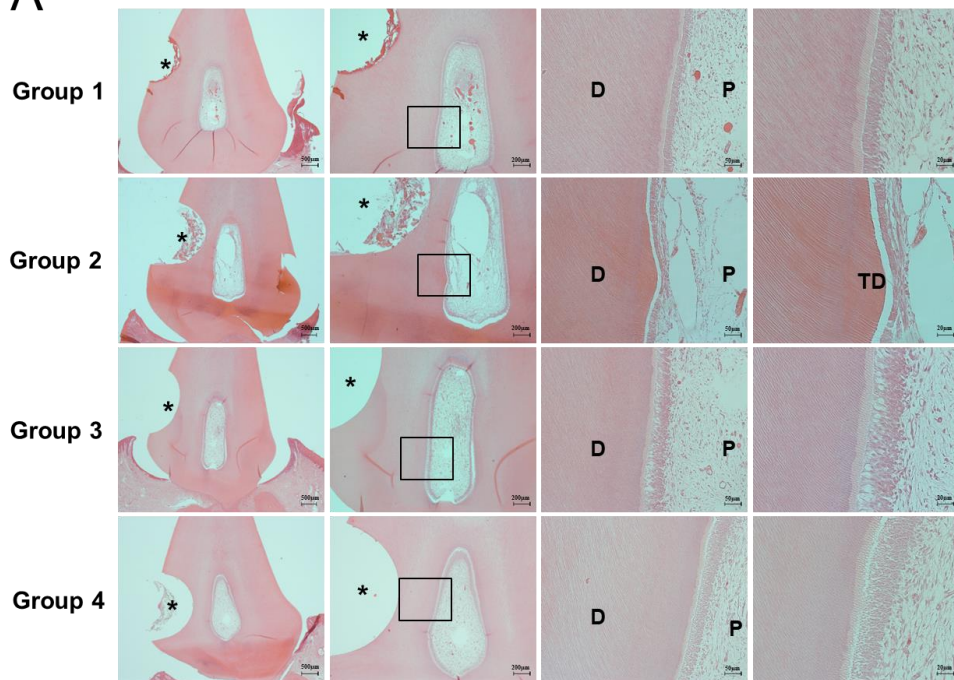
B
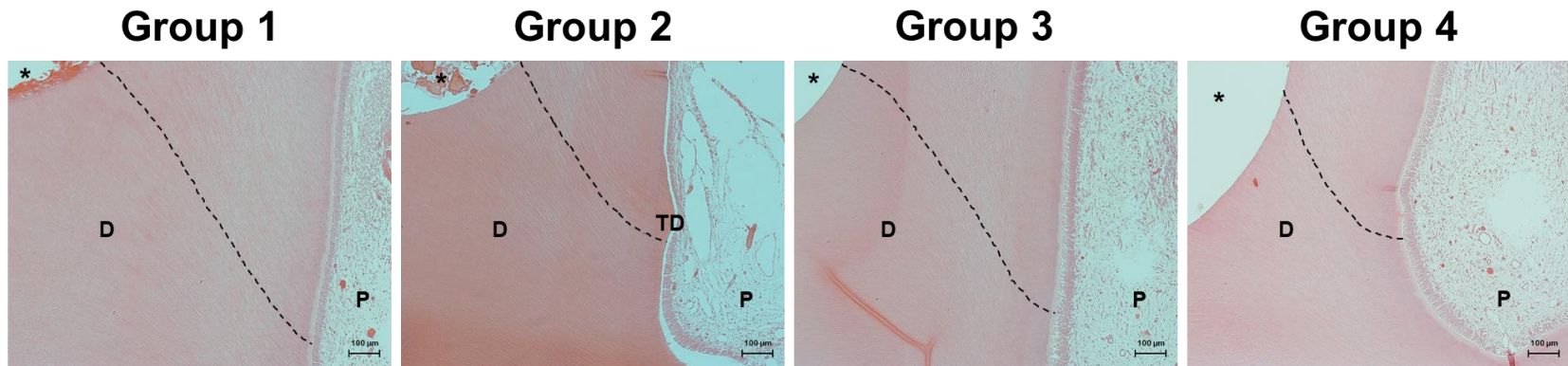
Figure 3. Histologic analysis after application of various toothpastes in the dentin hypersensitivity model with canine teeth. The toothpastes were applied using the bass method to all groups of teeth, once daily for 6 weeks. In groups 1, 3, and 4, no histologic changes were observed in the dentin-pulp interface. In contrast, group 2 showed newly formed tertiary dentin. Boxed areas are shown at higher magnification. The asterisk indicates the defect area; D represents dentin; P represents pulp; TD represents newly formed tertiary dentin.

3.4. Comparison of permeability and sealing ability

The representative graphs of dentinal fluid flow according to time are presented in Figure 4. The negative control demonstrated a rapid increase in dentinal fluid flow over time because the dentinal tubules were fully open. In groups 1, 3, and 4, the dentinal fluid flow progressively increased because the dentinal tubules were partially occluded. Subsequently, a statistical analysis was performed using the volume of the dentinal fluid flow at 1020 sec. In comparison to the negative control, all groups presented noticeably reduced dentinal fluid flow. The volume of dentinal fluid flow was significantly smaller in group 2 than in group 1, although the dentinal tubules were only partially blocked, according to the SEM images of the dentin surface. On the other hand, the volume of dentinal fluid flow in group 3 and 4 did not differ significantly compared to that of group 1. These results indicate that the CPNE7-DP-containing toothpaste had a better dentin sealing effect than did the toothpaste of group 1.
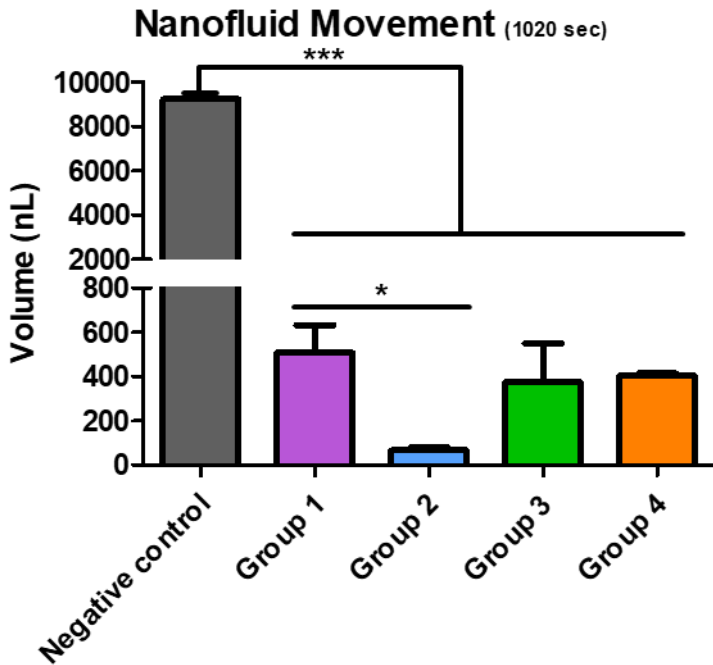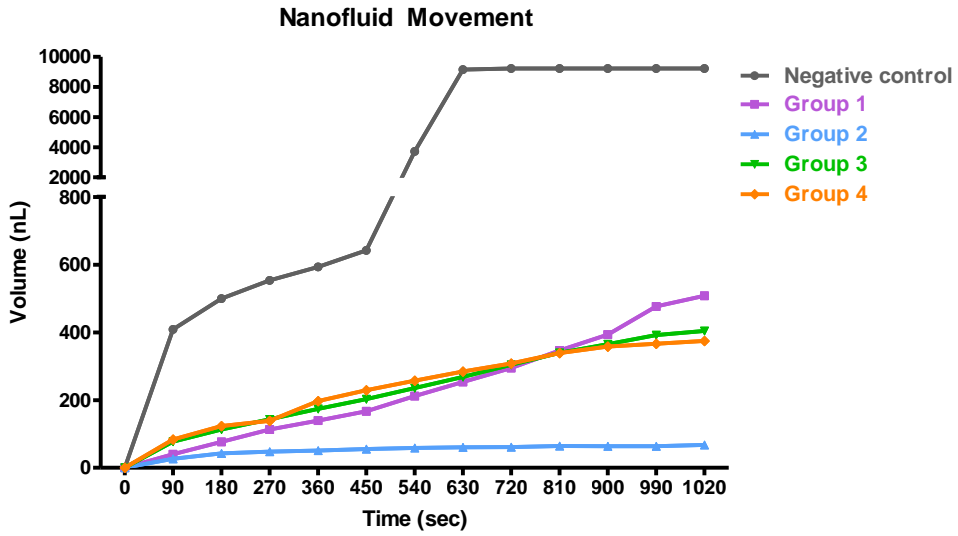
Figure 4. Representative graphs of dentinal fluid flow after application of various toothpastes. This flow progressively increased in groups 1, 3, and 4; that of group 2 was significantly lower than that of the group 1. (*p< 0.05 and ***p <0.001)

3 4

4. Discussion

This study demonstrated that CPNE7-DP increases the mitochondrial function of hDPCs under oxidative stress, and CPNE7-DP containing toothpastes induces tertiary dentin formation and dentin sealing effects in a hypersensitivity model. Due to exposure to numerous stimuli, the oral cavity is a location where ROS can easily build (Zukowski et al. 2018). Mitochondrial function is closely related to the regulation of ROS levels (Brand et al. 2004; Chih-Hung and Pei-Chung 2012; Venditti et al. 2013). H_2O_2, one of the ROS, can diffuse across membranes and react with metal ions to form hydroxyl radicals. Since only a few antioxidants can neutralize the hydroxyl radical, it is the most harmful and reactive free radical in the living systems (Halliwell et al. 2000; Halliwell and Gutteridge 2015).

Odontoblasts are long-lived post-mitotic cells. In mature odontoblasts, reduced intracellular organelles and debilitated cellular function such as decreased dentin-secretory activity are observed due to aging(Couve et al. 2013). The aging process leads to the damaged mitochondria that produce less ATP and accumulate more ROS (Barja 2013; Lopez-Otin et al. 2013). Furthermore, damaged mitochondria are known to cause dysfunctional odontoblasts (Imhof et al. 2020; Matsuishi et al. 2018). Therefore, considering that Age-related accumulation of ROS and mitochondrial dysfunction are present in mature odontoblasts,

enhancing the mitochondrial function of mature odontoblasts is required to improve cellular function. This study shows that CPNE7-DP significantly increased maximal mitochondrial respiration in H_2O_2-treated hDPCs. These results implicate that CPNE7-DP is involved in mitochondrial function in hDPCs.

The assessment of the efficacy of desensitizing toothpastes showed CPNE7-DP- containing toothpaste can induce tertiary dentin formation to promote a sustained dentin sealing effect and act as a successful desensitizer. In this study, we compared the dentin sealing effect of CPNE7-DP- containing toothpaste and two commercially available toothpastes and investigated permanent changes, such as tertiary dentin formation. The group 1 (control) and group 2 (CPNE7-DP-containing toothpaste) have identical components except CPNE7-DP. These finding implies that CPNE7-DP causes the tubular dentin formation and dentin sealing effect. The group 3 and group 4 are commercially available desensitizing toothpastes with different manufacturers, and their ingredients and contents are not completely disclosed. Therefore, it is difficult to clearly compare the difference in ingredients except the active ingredient between other groups. However, no hard tissue formation was observed *in vivo* hypersensitivity model in both groups 3 and 4. Moreover, dentinal fluid flow was not significantly different from group 1 without active ingredients. Based on these results, it is considered that the research findings were unaffected by the different ingredients.

In the SEM analysis, tubule occlusion was observed in all

experimental groups but not in the negative control group; however, not all open dentinal tubules were completely occluded. In addition, we observed a little difference in the tubule occlusion between disks brushed for 2 weeks and those brushed for 4 weeks. Even in group 1, which did not contain desensitizing ingredients, dentinal tubule occlusion was observed. SEM image analysis *in vitro* hypersensitivity model is one of the methods mainly used to evaluate the efficacy of desensitizing toothpastes. However, because the SEM images depicted only the tooth surface, SEM may be insufficient for the evaluation of the entire dentin sealing effect.

In contrast, distinct differences between the groups were observed in the histological analysis and microleakage analysis in the *in vivo* hypersensitivity model. In group 2, in which the CPNE7-DP-containing toothpaste was used, the dentinal fluid flow was significantly decreased in comparison with group 1 as well as the negative control. Of more importance is that we observed newly formed tertiary dentin with tubular structure in group 2 of the dogs' teeth but no such change in the other groups.

CPNE7-DP, a synthetic oligopeptide derived from CPNE7 protein, was studied in previous research. Lee et al. demonstrated that CPNE7-DP was noncytotoxic, induced odontoblast differentiation *in vitro*, and induced regeneration of tubular dentin in models with shallow and deep cavities. In addition, they confirmed that peritubular dentin formation was induced by the CPNE7-DP treatment in the model of beagle tooth defects to promote dentinal tubule occlusion, and the volume of the dentinal fluid flow was

significantly reduced (Lee et al. 2020). These findings—less dentinal fluid flow and newly formed tertiary dentin—were essentially in agreement with the results in group 2 of this study. Therefore, we suggest that the use of toothpaste containing CPNE7-DP can cause permanent changes, such as tertiary dentin formation, which would result in long-term dentin sealing effects.

In the toothpaste used in group 3, calcium carbonate and arginine were active ingredients. The combination of these two substances forms a positive complex with the negatively charged dentin surface, which facilitates tubular occlusion (Kleinberg 2002). Other studies have demonstrated that ions of strontium acetate, the active ingredient of the toothpaste used in group 4, were exchanged with calcium ions, which caused the formation of strontium crystals within dentinal tubules; thus, strontium can cause occlusion of dentinal tubules (Kun 1976; Mishima et al. 1995; Olley et al. 2015). Therefore, we speculate that partial tubule occlusion occurred in groups 3 and 4 as a result of the action of these active ingredients. In addition, calcium carbonate is able to induce *in vitro* cell differentiation of human dental pulp stem cells into odontoblasts (Hirayama et al. 2013), and strontium at specific doses could influence proliferation, odontogenic differentiation, and mineralization of human dental pulp stem cells in vitro via the calcium-sensing receptor (Huang et al. 2016). Nevertheless, in this study, hard tissue formation was not observed in groups 3 and 4, in which toothpaste containing calcium carbonate and strontium acetate, respectively, was used.

There are some limitations in this study. This study is a lack of data showing that CPNE7-DP changes odontoblast activity or mineralization markers by increasing mitochondrial function. To better understand the relationship between CPNE7, odontoblast, and mitochondria, further studies are needed. Additionally, it would have been helpful to have a control group of random peptides as this study used CPNE7-DP. Although not in this study, random peptide was used in the previous study and did not have any effects including tertiary dentin formation (Lee et al. 2020). Moreover, future research is required to evaluate the stability of CPNE7-DP–containing toothpaste in a dietary acid challenge.

Altogether, this study suggests the possibility that CPNE7-DP can induce tertiary dentin formation by enhancing mitochondrial function of hDPCs under oxidative stress. Additionally, an analytical method is proposed for precise evaluation and understanding of therapeutic agents for dentin hypersensitivity. Our findings have important implications for the use of CPNE7-DP as a novel biological active ingredient in the treatment of dentin hypersensitivity. Ultimately, treatment with CPNE7-DP–containing toothpaste for dentin hypersensitivity may offer a new and fundamental way with a low risk of recurrence and little microleakage. Furthermore, CPNE7-DP has the potential for being used widely in combination with dental materials in clinical practice.

Part 2.

Copine7 deficiency leads to hepatic fat

accumulation via mitochondrial dysfunction

1. Introduction

1.1 Non-alcoholic fatty liver disease (NAFLD)

Non-alcoholic fatty liver disease (NAFLD), a chronic liver disorder, is one of the most prevalent metabolic diseases and a public health concern worldwide (Chalasani et al. 2012; Than and Newsome 2015). According to published studies, the global NAFLD prevalence was 29.8% and has continued to increase (Le et al. 2021). NAFLD, which is generally diagnosed through radiological imaging techniques, is defined as a fat accumulation of 5% or more in the absence of significant alcohol intake (Byrne and Targher 2015; Chalasani et al. 2012). NAFLD ranges from simple steatosis to steatohepatitis. Simple steatosis refers to the presence of fat accumulation of at least 5% without any inflammation. Steatohepatitis (NASH) is defined as inflammation with hepatocellular damage such as hepatocyte ballooning and the presence of fat accumulation of at least 5% (Chalasani et al. 2018). NAFLD can progress to liver fibrosis, cirrhosis, and, ultimately, hepatocellular carcinoma (Chalasani et al. 2012; Neuschwander-Tetri 2010). It has been reported that the progression of NAFLD also increases the risk of liver disease-related mortality (Ekstedt et al. 2006; Matteoni et al. 1999; Musso et al. 2011). However, there is no approved treatment for NAFLD to date. Therefore, it is necessary to better understand the pathological mechanism of NAFLD and to develop therapeutic targets.

1.2 The pathogenesis of NAFLD

The pathogenesis of NAFLD has not been fully elucidated and is usually explained by the "multiple hit" hypothesis. NAFLD is caused by a combination of factors such as nutritional factors, genetic and epigenetic factors, insulin resistance, lipid metabolism dysregulation, gut microbiota, oxidative stress and mitochondrial dysfunction (Buzzetti et al. 2016). NAFLD is mainly characterized by lipid metabolic disorder, and hepatic lipid is produced by the influx of fatty acids through *de novo* lipogenesis, adipose tissue lipolysis, and reabsorption in circulation (Bugianesi et al. 2010; Kirpich et al. 2015). Hepatic lipids are removed through the beta-oxidation of fatty acids in mitochondria and their release into very-low-density lipoprotein (VLDL) (Ferramosca and Zara 2014).

1.3 Mitochondrial dynamics

Mitochondria are essential organelles that play a vital roles in cell biology by producing energy through fatty acid beta-oxidation, the tricarboxylic acid cycle, and oxidative phosphorylation (Pessayre et al. 1999). Mitochondria orchestrate numerous essential biosynthetic and metabolic pathways, as well as apoptosis, calcium, and redox homeostasis (Ernster and Schatz 1981; Rizzuto et al. 2000; Scorrano 2009). Mitochondria are highly dynamic and continuously change shape as a result of fusion and fission processes (Yu et al. 2020). Mitochondrial dynamics are involved in the quality control mechanism that maintains mitochondrial function

(Chan 2020; Giacomello et al. 2020). Mitochondrial morphology can be modulated by the structural components and signaling pathways (Giacomello et al. 2020). Changes in mitochondrial morphology help mitochondria adapt to specific cellular and tissue demands and regulates mitochondrial reaction to cytosolic signals (Pernas and Scorrano 2016). Therefore, mitochondrial fusion and fission are key events regulating normal mitochondrial function and prevent disease (Chen et al. 2015).

Mitochondrial fusion is mediated by two mitofusins (MFN1 and MFN2) and optic atrophy1 (OPA1). MFN1 fuse the inner mitochondrial memgrane (IMM) with OPA1 and the outer mitochondrial membrane (OMM) with MFN2 (Chen et al. 2003; Koshiba et al. 2004). In addition, MFN2 participate in tethering mitochondrion to mitochondrion and mitochondria to other organelles (de Brito and Scorrano 2008; Ishihara et al. 2004).

Mitochondrial fission is primarily regulated by dynamin-related protein 1 (DRP1), mitochondrial fission factor (MFF) and mitochondrial fission 1 protein (FIS1). DRP1 oligomerizes and drive fragmentation (Mears et al. 2011). FIS1 and MFF functions as a DRP1 receptors to recruit DRP1 (Karren et al. 2005; Otera et al. 2010).
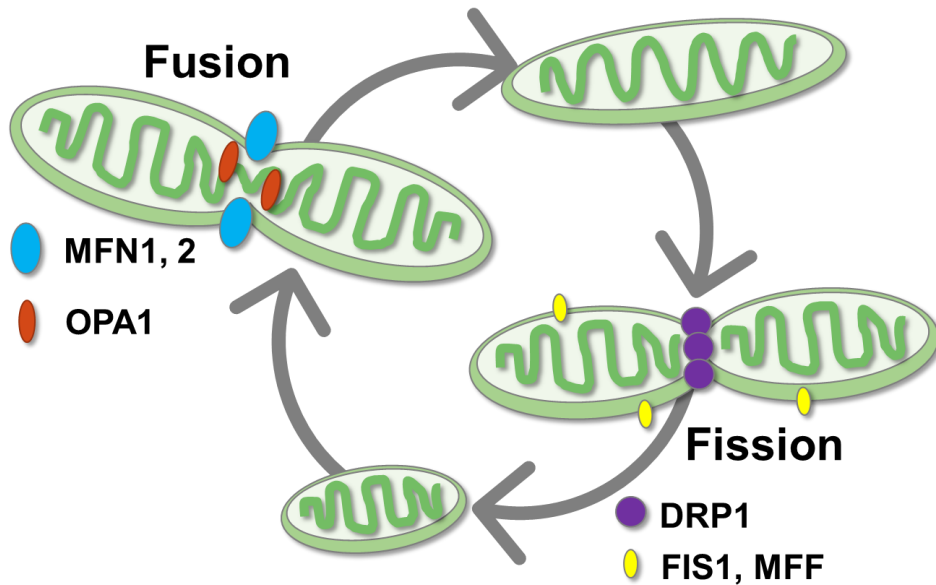
Schematic representation of mitochondrial dynamics. Mitochondria are dynamic organelles in which fission and fusion occur continuously. MFN1, 2: mitofusin 1, 2; OPA1: optic atrophy 1; DRP1: dynamin-related protein 1; FIS1: Mitochondrial fission 1; MFF: mitochondrial fission factor.

1.4 Mitochondrial dysfunction in NAFLD

The liver is one of the most mitochondrial-rich tissues, and there are between 500 and 4000 mitochondria per hepatocyte (Degli Esposti et al. 2012). Metabolic stressors or genetic variants can be responsible for mitochondrial dysfunction. Mitochondrial dysfunction contributes to NAFLD pathogenesis and progression by affecting hepatic lipid homeostasis and promoting reactive oxygen species (ROS) generation and lipid peroxidation (Begriche et al. 2006; Mansouri et al. 2018; Rector et al. 2010). Indeed, previous studies have shown that mitochondrial ultrastructural abnormalities,

defective dynamics, and high ROS levels were observed in NAFLD patients (Ibdah et al. 2005; Rector et al. 2013; Sanyal et al. 2001). Moreover, in terms of the mitochondrial morphology, the increased hepatic mitochondrial mass in NAFLD patients was confirmed, which may be the result of the defective removal of damaged mitochondria (Mansouri et al. 2018). Therefore, the maintenance of mitochondrial dynamics and function is crucial for hepatic lipid metabolism and integrity.
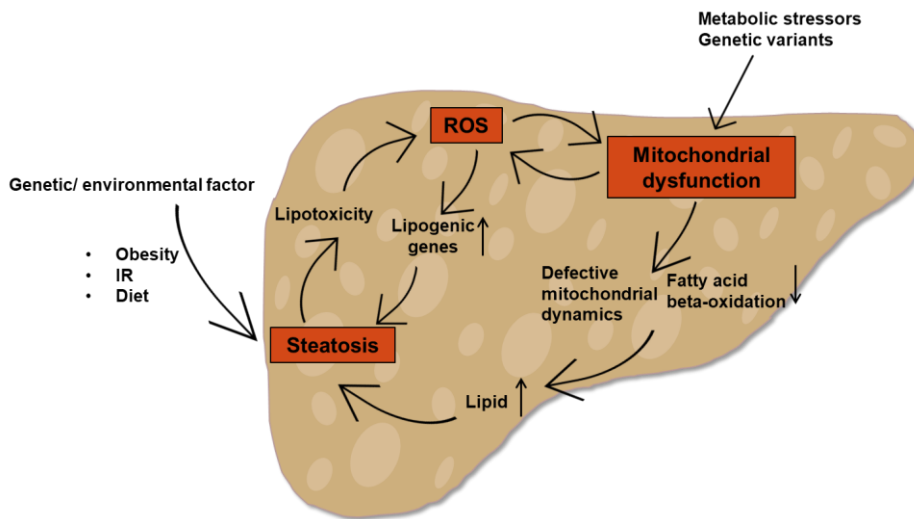
Schematic depiction of mitochondrial dysfunction in NAFLD. Mitochondrial dysfunction contributes to NAFLD pathogenesis and progression by affecting lipid metabolism and promoting reactive oxygen species (ROS) formation.

1.5 Copines in lipid metabolism

Copines (CPNE) are a Ca^{2+}-dependent phospholipid-binding protein family that has two C2 domains (C2A and C2B) and one von Willebrand factor A domain.(Creutz et al. 1998) The C2 domain is involved in Ca^{2+}-dependent phospholipid binding, and the von Willebrand factor A domain is known to mediate protein-protein interactions by binding to the tetratricopeptide repeat domain (Nalefski and Falke 1996). Copines exist ubiquitously in most eukaryotes, except yeast and Drosophila, and are generally present as a family of multiple homologs (Creutz et al. 1998). The high degree of conservation and multiplicity of this copine family suggests that copines play a fundamental role in cell biology.

Recent studies have consistently reported that the copine family is associated with the lipid metabolic pathway. Wang et al. reported that genetic variants of *CPNE5* were associated with obesity (Wang et al. 2015). Additionally, Tan et al. reported that the low expression of *CPNE3* is associated with the risk of acute myocardial infarction in patients with stable coronary artery disease (Tan et al. 2019). Moreover, Zhou et al. reported that the gene variant of *CPNE7* was associated abnormalities in fatty acid and lipid metabolism through whole-exome sequencing and genome-wide association studies (Zhou et al. 2019). However, the function of *Cpne7* in the liver, which is the central organ of lipid metabolism, has not yet been elucidated. Further, studies on *Cpne7* in mitochondria, which are abundantly present in the liver and are the major organelle of fatty acid oxidation, have not yet been conducted.

1.6 Purpose of research

Considering the findings of previous studies, it is indispensable to investigate the relationship between lipid metabolism and *Cpne7*. Therefore, this study aims to explore the role of *Cpne7* in hepatic fat accumulation.

2. Materials and Methods

2.1. Animals

All animal procedures were approved by the Institutional Animal Care and Use Committee of Seoul National University (SNU-210208-4-1). This study also conformed to the ARRIVE guidelines and was performed in accordance with the National Research council's Guide for the Care and Use of Laboratory Animals. C57BL/6 mice were purchased from Dooyeol Biotech (Seoul, Korea), and the *Cpne7*-null (*Cpne7*$^{-/-}$) mice were created by deleting Exons 5, 6, and 7 of the *Cpne7* gene through the gene targeting system and cloning a vector containing EGFR and NeoR. The cloned vector was transformed using the electroporation method in the CMTI-1 ES cell line derived from 129/SVEV mice. After electroporation, G418/ganciclovir-resistant colonies were selected and transplanted into surrogate mothers to generate offspring. *Cpne7*$^{-/-}$ mice were identified by PCR. The primers used were exon7 F (5'-CAGAAGGCCTTTGAGGAGGAGC-3', deleted region), neo F (5'-CAA TATGGGATCGGCCATTGAAC-3', *Cpne7*$^{-/-}$ vector sequence) and exon8 RR (5'-GTTTGTACTTGGCAT TCACACAGTCC-3'). The *Cpne7*-overexpressing transgenic (*Cpne7* Tg) mice were prepared using the same method as in the production of the *Cpne7*$^{-/-}$ mouse after constructing a vector using the keratin-14 (K14) promoter to overexpress epithelial cells specifically by Macrogen. *Cpne7* Tg

mice were identified by PCR. The primers used were *K14* F (5' −
CACGATACACCCGACTAGCT−3') and Cpne7 R (5' −
CTAGGAAGTCATCATCCTGGC−3'). Experiments were
performed on male mice. All mice used in the experiment were
housed in cages with a 12:12−hour light/dark cycle at about 20° C
−25° C and 45%−55% humidity.

2.2. RNA−sequencing analysis

Total RNA was extracted from homogenized liver tissues of 1−
month−old wild−type (WT) and *Cpne7*$^{-/-}$ mice (n = 3) using the
TRIzol reagent per the manufacturer's instructions (Invitrogen,
Carlsbad, CA, USA). The total RNA (2μg) of each group was
shipped in a freezing container to Macrogen. RNA−seq library
construction was performed using the TruSeq Stranded mRNA LT
Sample Prep Kit (Illumina, San Diego, CA, USA). cDNA libraries
were produced via the purification of total RNA, random
fragmentation, and reverse transcription into cDNA. The libraries
were sequenced using the NovaSeq 6000 system (Illumina). After
sequencing the libraries, the quality control of raw reads obtained
through sequencing was performed. It produced basic statistics
such as overall read quality, total bases, total reads, and GC (%). In
order to reduce the bias of the analysis result, a pre−processing
process was conducted by removing low−quality or artifacts such
as adapter sequence, contaminant DNA, and PCR duplicates. The
pre−processed trimmed reads were mapped to the reference
genome using the HISAT2 program, followed by generation of

aligned reads. After read mapping, the transcript assembly was performed through the StringTie program. Expression profile values were obtained for each sample for the known transcript and read count and Fragment per Kilobase of transcript per Million mapped reads (FPKM) values were summarized based on transcript/gene. Using this value, differentially expressed gene (DEG) analysis was performed using FPKM for the comparative combination. In order to select genes differentially expressed between the two groups, genes that satisfied conditions which are |fold change (FC)|>=2 and raw p-value <0.05 of independent t-test were extracted. Through hierarchical clustering (Euclidean Distance, Complete Linkage) analysis for significant genes, the grouped information of samples and genes was visualized using the degree of similarity of expression patterns for each gene in each sample. For the list of significant differentially expressed genes (DEGs), the Gene set enrichment analysis in a biological process and molecular function, was performed using gProfiler (https://biit.cs.ut.ee/gprofiler/orth). The functional protein association networks were conducted using String database (https://string-db.org).

2.3. HFD-induced NAFLD model

The control WT, $Cpne7^{-/-}$, and $Cpne7$ Tg mice (n = 6) were fed a chow diet (CD; 2018s, Envigo, Udine, Italy). For NAFLD induction, the experimental WT, $Cpne7^{-/-}$, and $Cpne7$ Tg mice (n = 6) were fed a 60% high-fat diet (HFD; TD.06414, Envigo). The HFD was performed on 6-week-old male mice for 16 weeks. After

CD or HFD feeding for 16 weeks, the mice were anesthetized with a 2.5% 2-methyl-2-butanol (Avertin; 240486, Sigma-Aldrich, MO, USA) solution diluted with RNase-free water (BWA-8000, T&I, Korea). Subsequently, the body and liver weights were measured, and a macroscopic analysis of the body and liver was conducted.

2.4. Serum analysis

The mice (n = 4) were anesthetized, and blood samples were collected via cardiac puncture after overnight fasting prior to their sacrifice. The whole blood was centrifuged at 2000 g for 10 min to obtain serum. The obtained serum was shipped in freezing containers to GCCL (Yongin, Korea). The serum levels of albumin (g/dL), alanine aminotransferase (ALT; U/L), total cholesterol (T. col; mg/dL), triglyceride (TG; mg/dL), free fatty acid (FFA; μEq/L), and glucose (mg/dL) were measured through GCCL.

2.5. Dual-energy x-ray absorptiometry (DXA)

The mass and percentages of body fat, bone mineral contents, lean were measured via DXA (InAlyzer, Medikors, Korea). After being fed the CD or HFD, experimental mice of each group (n = 6) were anesthetized and positioned at the center of the InAlyzer scanning area. After image scanning, representative images and measurements were acquired using the InAlyzer software program.

2.6. Hematoxylin and eosin (H&E) staining

The harvested tissues (n = 6) were fixed in 4% paraformaldehyde in PBS at 4 ˚C for a day. Subsequently, dehydration, clearing, and paraffin infiltration were performed using an automatic tissue processor (TP 1020, Leica, Wetzlar, Germany). The tissues were embedded in paraffin and sectioned into 5-μm-thick slices using a microtome (RM 2155, Leica, Wetzlar, Germany). After deparaffinization and rehydration, these sections were stained with H&E, dehydrated, cleared, and mounted.

For steatosis quantification, the void area occupied by lipid infiltrates in the H&E-stained images at ×400 was analyzed using the particle analysis of Image J (National Institute of Health, USA). To exclude central veins and liver sinusoids, the size of the measurement range was set to 20-5000 $μm^2$, and the circularity was set to 0.5-1.0. The percentage of steatosis is the ratio of area covered by lipids to total area.

2.7. Transmission electron microscopy (TEM) analysis

The harvested tissues were fixed in Karnovsky's fixative at 4 ˚C for 4 hours. Subsequently, the tissues were post-fixed in 1% osmium tetroxide diluted in 0.1-M sodium cacodylate buffer. After *en bloc* staining with 0.5% uranyl acetate, dehydration was performed using a graded ethanol series and propylene oxide, and the infiltration of Spurr's resin was conducted. The polymerized blocks were sectioned using an ultramicrotome (Leica, EM UC6). TEM images were obtained using JEM-1400 Flash.

2.8. Measurement of ROS levels

ROS levels were analyzed using a ROS assay kit (ab113851, Abcam, Cambridge, UK). The ROS assay was performed per the manufacturer's instructions. Deparaffinized tissue sections were incubated with the 2, 7-Dichlorofluorescin diacetate (DCFDA) solution for 45 mins at 37 °C in the dark. After being washed, the tissue sections were stained with 4', 6-diamidino-2-phenylindole (DAPI) for five mins. Subsequently, the mounting procedure (s3023, DAKO, Copenhagen, Denmark) was conducted. ROS levels of tissue sections were measured via confocal laser scanning microscopy (CarlZeiss, LSM 800) at Ex/Em = 485/535 nm.

The cells were seeded 96-well microplates with 25,000 cells per well. After incubation overnight, the cells were stained by adding the DCFDA solution for 45 mins at 37 °C in the dark. Subsequently, the DCFDA solution was removed and H_2O_2 (1mM) was treated for four hours. The plates were measured on a fluorescence plate reader at Ex/Em = 485/535 nm.

2.9. Western blot

Western blotting was performed as previously described (Seo et al. 2017). Liver tissue samples were homogenized using ice-cold RIPA buffer with a homogenizer (SuperFastPrep-2, #6012500, MP Biomedicals, USA). The cells were lysed using ice-cold RIPA buffer. The liver homogenates and lysed cells were centrifuged at 13,000 rpm for 30 min, and the supernatant was collected. Proteins (5-40 μg) were loaded into the polyacrylamide gel and probed

primary antibody. Primary antibodies used for western blots were as follows: Anti-DRP1 (1:1000, sc-271583, Santa Cruz Biotechnology; Santa Cruz, CA, USA), anti-MFF (1:500, sc-398617, Santa Cruz Biotechnology), anti-FIS1 (1:500, sc-376447, Santa Cruz Biotechnology), anti-MFN1 (1:500, sc-166644, Santa Cruz Biotechnology), anti-MFN2 (1:500, sc-100560, Santa Cruz Biotechnology), and anti-GAPDH(1:20000, CSB-RA009232A0HU, CUSABIO, Houston, TX, USA). Anti-CPNE7 were produced as previously described (Lee et al. 2011). After incubation with the secondary antibody, protein loading was measured by the expression of GAPDH. Secondary antibodies used were as follows: anti-rabbit (GTX213110-01, Genetex, California, USA) or anti-mouse (GTX213111-01, Genetex) immunoglobulin G conjugated to horseradish peroxidase secondary antibodies (1:5000). Semi-quantitative assessments were conducted using Image Studio Lite (Version 5.2, Li-cor, Lincoln, NE, USA).

2.10. Cell culture and transfection

The HepG2 cell line was purchased from the Korea Cell Line Bank (Seoul, Korea, KCLB no.88065). HepG2 cells were grown and maintained in MEM (Gibco BRL, Carlsbad, CA, USA) supplemented with 10% FBS (Gibco BRL) and antibiotic-antimycotic reagents (Gibco BRL) at 37 ° C in a humidified 5% CO_2 atmosphere.

The expression vector encoding DDK (Flag)-tagged *CPNE7* (NM_153636) was purchased from Origene (Rockville, MD, USA). Control shRNA (sc-37007) and *CPNE7* shRNA (sc-93065-SH)

were purchased from Santa Cruz Biotechnology. The HepG2 cells were seeded in 60 mm culture dishes at a density of 5×10^5 cells per well. The cells were transfected with DDK (Flag)-tagged *CPNE7* and sh*CPNE7* using the Metafectene Pro reagent (Biontex, Marinsried, Germany) per the manufacturer's instructions.

2.11. Measurement of mitochondrial function

Oxygen consumption rate (OCR) was measured by Seahorse XFe96 Extracellular Flux Analyzer with XF Cell Mito Stress Test Kit as per manufacturer's protocol (Seahorse Bioscience, North Billerica, MA, USA). Briefly, HepG2 cells were treated using H_2O_2 (200 μM, 24h) following transfection of control, shCPNE7 and CPNE7 o/e and were seeded at a density of 2×10^4 cells/well onto 96-well cell culture plate for overnight. The medium was replaced the following day to XF running medium with 2 mM L-glutamine and 1000 mg/L D-glucose for OCR measurement. Cells were sequentially exposed to Oligomycin (1.5 μM; ATPase inhibitor), FCCP (0.5 μM; mitochondrial uncoupler) and Rotenenone/Antimycin A (0.5 μM; complex I/III inhibitor). The average measurement from experiments conducted in triplicate is shown by each point in the traces.

2.12. Oil-red O staining

After treatment with H_2O_2 (200 μm) for 24 h, HepG2 cells were fixed in 10% formalin (Junsei Chemical, Japan) for 30 mins. After being washed, the cells were incubated in 60% isopropanol (Duksan,

Korea) for 5 mins and covered in the oil-red O solution (Sigma-Aldrich) for 20 mins. After being washed, the cells were counterstained using hematoxylin for 1 min and washed with distilled water, followed by viewing under a microscope. For quantification, after staining with hematoxylin and washing, the cells were washed using 60% and 100% isopropanol, and then the supernatant was used to read the absorbance at 492 nm.

2.13. Statistical Analysis

Statistical analyses were performed using GraphPad Prism software (version 5, GraphPad Software, CA, USA). All values are expressed as the mean ± standard deviation for at least three independent experiments. Between-group statistical analyses were performed using the one- or two-way analysis of variance followed by Tukey's or Bonferroni's post- hoc test, respectively. Statistically significant differences between groups were considered at *p < 0.05, **p < 0.01 and ***p < 0.001.

3. Results

3.1. *Cpne7* deficiency is associated with hepatic fatty changes.

To investigate whether *Cpne7* is involved in hepatic lipid metabolism, histological analysis was conducted in the livers of WT and *Cpne7*$^{-/-}$ mice. In the H&E-stained images, numerous LDs were observed in the livers of *Cpne7*$^{-/-}$ mice compared with WT mice (Figure 5). This result suggests that *Cpne7* is linked to hepatic lipid metabolism.
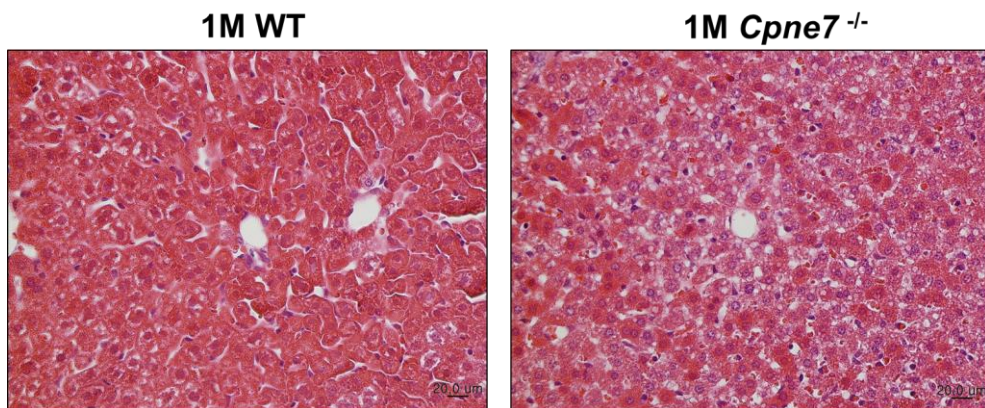

Figure 5. Numerous lipid droplets are observed in the livers of *Cpne7*$^{-/-}$ mice. H&E-stained images in the livers of 1-month-old WT and *Cpne7*$^{-/-}$ mice (scale bars = 20 μm).

3.2. *Cpne7* deficiency is involved in dysregulated lipid metabolism and mitochondrial dysfunction in RNA-sequencing analysis of liver tissues

To determine the difference in lipid metabolism-related gene expression, RNA-sequencing was performed in liver tissues of WT and *Cpne7*$^{-/-}$ mice (n = 3). The RNA-seq datasets can be found in online repositories. The names of the repository/repositories and accession number(s) can be found below: SRA PRJNA879973, https://www.ncbi.nlm.nih.gov/sra/PRJNA879973 As a result of RNA-sequencing, the significant gene expression pattern, as seen through the heat map, was different in the livers of WT and *Cpne7*$^{-/-}$ mice (Figure 6A). There were 178 upregulated genes and 171 downregulated genes in the livers of *Cpne7*$^{-/-}$ mice compared with those of WT mice on the condition of |fold change (FC)| ≥ 2. Among the genes, 135 genes were significantly increased, and 81 genes were significantly decreased in the livers of *Cpne7*$^{-/-}$ mice compared with those of WT mice (Figure 6B).

Subsequently, a Gene Ontology (GO) enrichment analysis targeting the list of significant DEGs was performed. The top 20 GO terms satisfying the p-value <0.05 for each category were presented as a dot plot. Most GO terms in the biological process were associated with lipid metabolism processes such as the lipid metabolic, lipid biosynthetic, fatty acid metabolic, and cholesterol metabolic processes (Figure 6C). The top GO terms in molecular functions were catalytic activity and oxidoreductase activity related to mitochondrial functions (Figure 6D).

The functional protein association networks were conducted using DEG list (Figure 6E). The line represents protein-protein associations. Each node (circles) represents all the proteins produced by a single, protein-coding gene locus. The node color indicates the corresponding GO terms. The interaction network showed that genes involved in lipid metabolism, fatty acid metabolism, insulin receptor signaling, and antioxidant activity were organically linked.

As can be seen in the DEG list related of lipid metabolism, sterol regulatory element binding transcription factor 1 (*Srebf1*), a transcription factor for lipogenesis, and downstream lipogenic genes were upregulated in the livers of *Cpne7*$^{-/-}$ mice compared with those of WT mice. Furthermore, fatty acid synthesis genes such as *Acot1, Acot11, Fabp2, Gpcpd1, Nudt7, Pex11a, Pex11a and Plcg1* were upregulated in the livers of *Cpne7*$^{-/-}$ mice compared with those of WT mice. Conversely, the leptin receptor (*Lepr*) and insulin-like growth factor-binding protein 1 (*lgfbp1*) were downregulated in the livers of *Cpne7*$^{-/-}$ mice compared with those of WT mice.

In the DEG list related of oxidoreductase activity, the expression of cytochrome P450 (Cyps) family, which is mostly found in the mitochondria and endoplasmic reticulum (ER), was altered. Additionally, NADPH oxidase 4 (*Nox4*), which causes oxidative stress, was upregulated and the genes with antioxidant activity such as *Mgst3, Nqo1, and S100a9* were downregulated in the livers of *Cpne7*$^{-/-}$ mice compared with those of WT mice (Table

3). These results indicate the possibility that *Cpne7* deficiency could affect hepatic lipid metabolism and mitochondrial function.

B

UP, DOWN regulated count
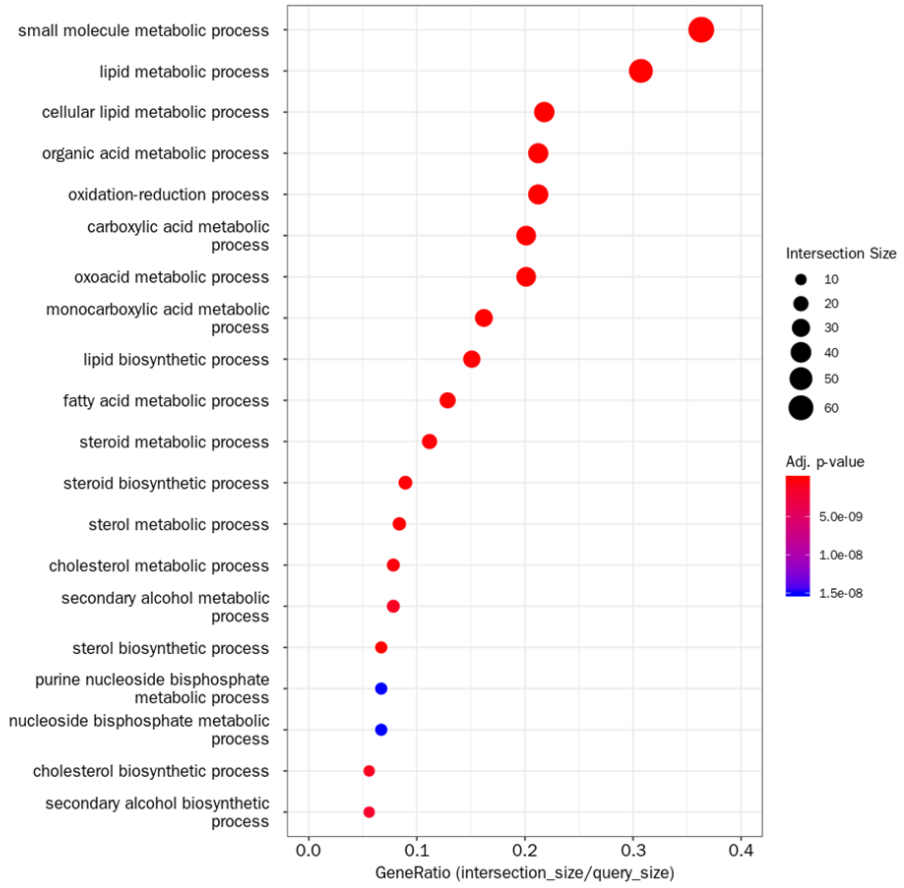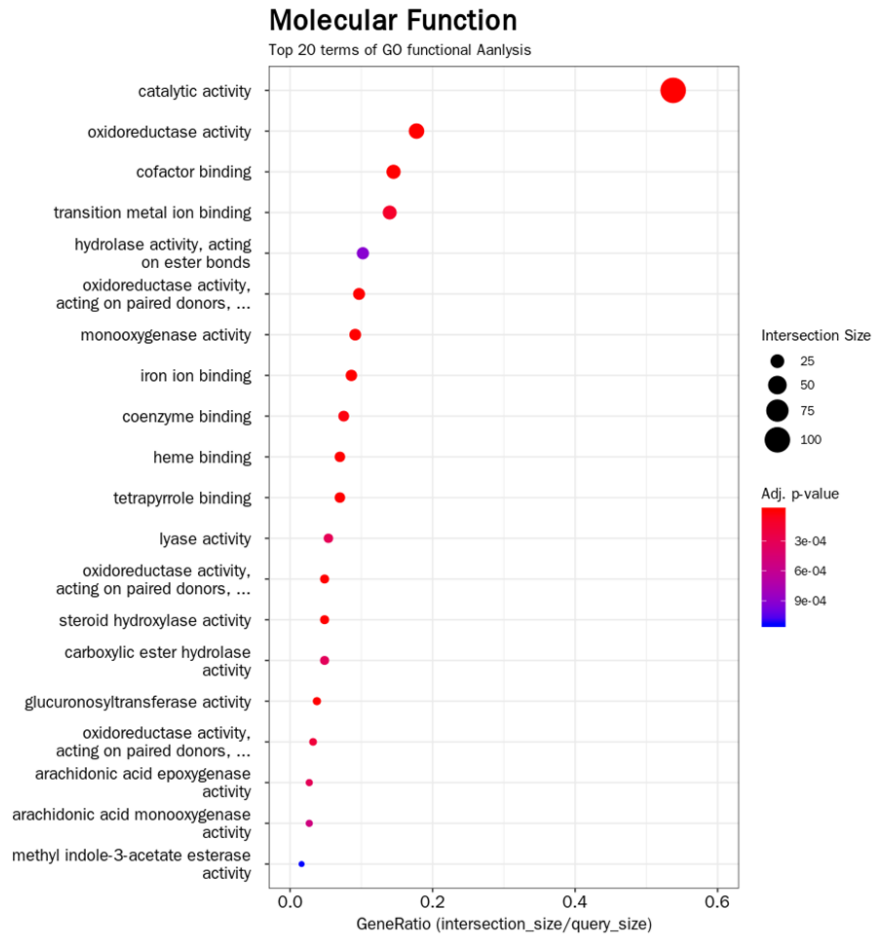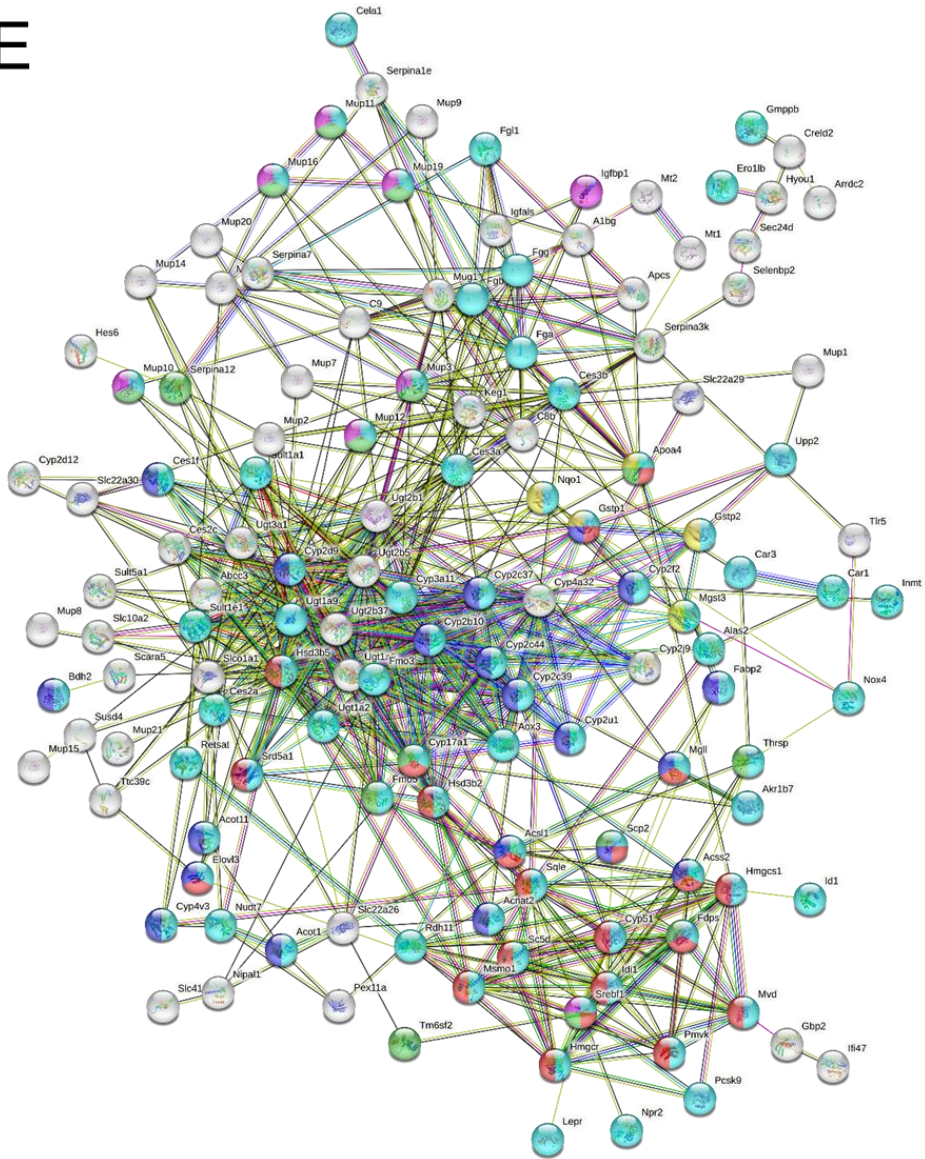(|FC|>=2)

UP, DOWN regulated count
(|FC|>=2 & raw.p<0.05)
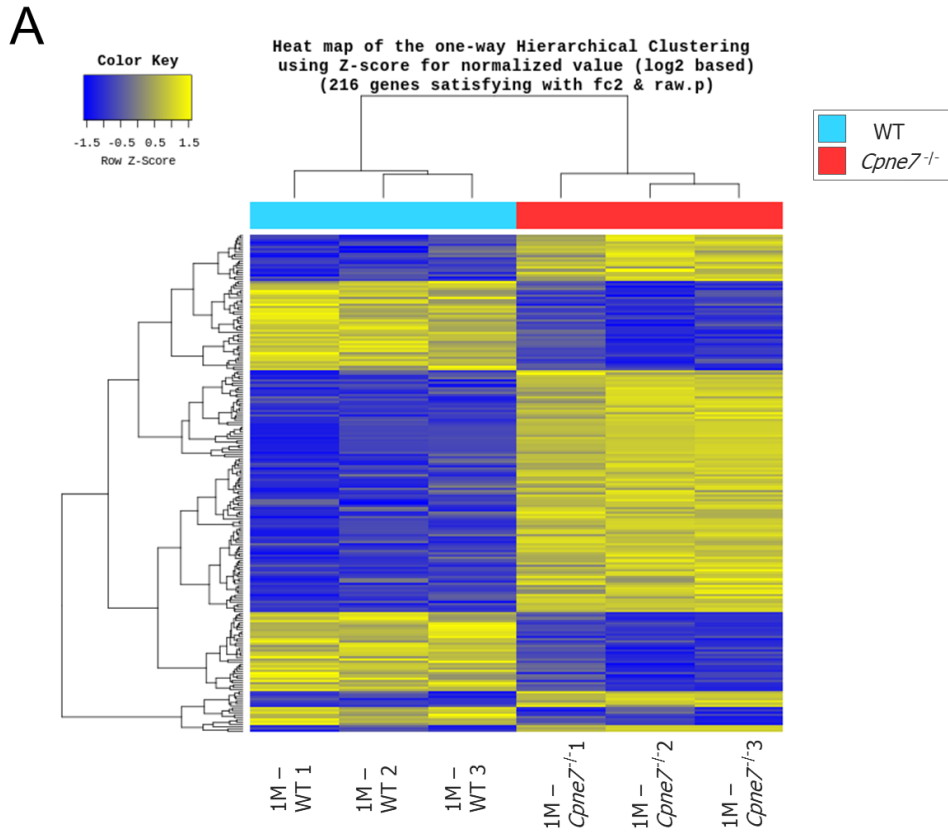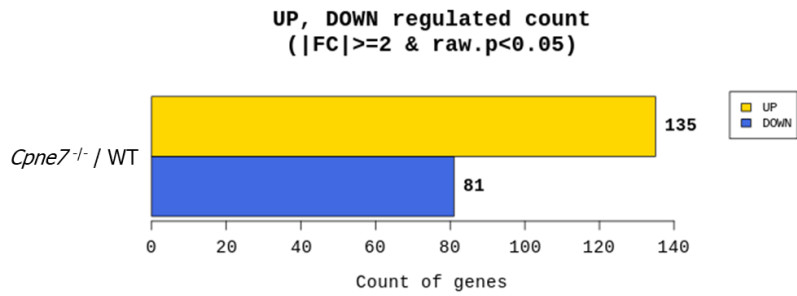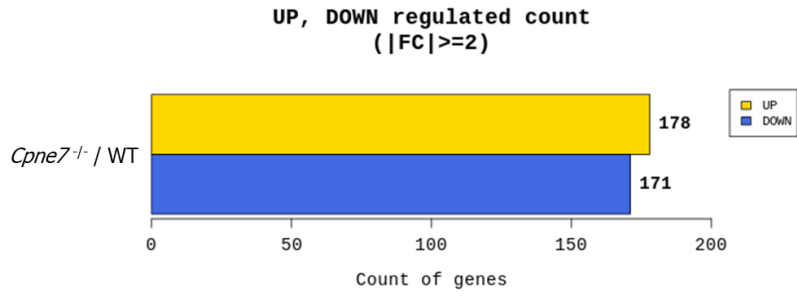
Biological Process
Top 20 terms of GO functional Aanlysis

D

Molecular Function

Top 20 terms of GO functional Aanlysis

E

Metabolic process
Lipid biosynthetic process
Fatty acid metabolic process
Regulation of lipid metabolic process
Insulin receptor signaling pathway
Antioxidant activity

Figure 6. Differentially expressed genes (DEGs) in the livers of *Cpne7*-null (*Cpne7*$^{-/-}$) mice are involved in dysregulated lipid metabolism and mitochondrial dysfunction in RNA-sequencing analysis. (A) Heat map for hierarchical clustering. The left column represents wild-type (WT) control, and the right column represents *Cpne7*$^{-/-}$ group. Each row represents a single gene. The color change from yellow to blue lg (FPKM+1) value ranging from high to low. (B) The number of DEGs by fold change (n=3). (C, D) GO functional analysis. (E) The functional protein association networks of DEGs.

Table 3. List of DEGs related to top GO terms

GO term	Gene	Description	KO/WT.fc
Lipid biosynthetic process *and* *fatty acid metabolism*	*Acot1*	acyl-CoA thioesterase 11	2.21
	Acot11	acyl-CoA thioesterase 11	2.05
	Acsl1	acyl-CoA synthetase long-chain family member 1	2.09
	Apoa4	apolipoprotein A-IV	2.04
	Elovl3	elongation of very long chain fatty acids-like 3	10.60
	Fabp2	fatty acid binding protein 2, intestinal	2.33
	Gpcpd1	glycerophosphocholine phosphodiesterase 1	2.29
	Hsd3b2	hydroxy-delta-5-steroid dehydrogenase, 3 beta- and steroid delta-isomerase 2	3.12
	Hsd3b5	hydroxy-delta-5-steroid dehydrogenase, 3 beta- and steroid delta-isomerase 5	64.31
	Igfals	insulin-like growth factor binding protein, acid labile subunit	2.24
	Mgll	monoglyceride lipase	2.34
	Mup12	major urinary protein 12	43.97

	Mup20	major urinary protein 20	29.57
	Nudt7	nudix (nucleoside diphosphate linked moiety X)−type motif 7	3.52
	Pex11a	peroxisomal biogenesis factor 11 alpha	2.16
	Plcg1	phospholipase C, gamma 1	2.07
	Scp2	sterol carrier protein 2, liver	2.20
	Serpina12	serine (or cysteine) peptidase inhibitor, clade A, member 12	4.91
	Srd5a1	steroid 5 alpha−reductase 1	8.45
	Srebf1	sterol regulatory element binding transcription factor 1	2.00
	Thrsp	thyroid hormone responsive	2.76
	Acnat2	acyl−coenzyme A amino acid N−acyltransferase 2	−3.31
	Acss2	acyl−CoA synthetase short−chain family member 2	−2.39
	Avpr1a	arginine vasopressin receptor 1A	−2.23
	Fdps	farnesyl diphosphate synthetase	−2.66
	Hacl1	2−hydroxyacyl−CoA lyase 1	−2.32
	Hmgcr	3−hydroxy−3−methylglutaryl−Coenzyme A reductase	−2.22
	Hmgcs1	3−hydroxy−3−methylglutaryl−Coenzyme A synthase 1	−5.68
	Idi1	isopentenyl−diphosphate delta isomerase	−2.70
	Igfbp1	insulin−like growth factor binding protein 1	−3.27
	Lepr	leptin receptor	−2.28
	Msmo1	methylsterol monooxygenase 1	−2.54
	Mvd	mevalonate (diphospho) decarboxylase	−2.69
	Plac8	placenta−specific 8	−2.17
	Pmvk	phosphomevalonate kinase	−3.15
	Sc5d	sterol−C5−desaturase	−2.39
	Sqle	squalene epoxidase	−2.57
Oxido−reductase activity	*Bdh2*	3−hydroxybutyrate dehydrogenase, type 2	2.25
	Cyp2b10	cytochrome P450, family 2, subfamily b, polypeptide 10	4.16
	Cyp2c44	cytochrome P450, family 2, subfamily c, polypeptide 44	3.13
	Cyp2d12	cytochrome P450, family 2, subfamily d, polypeptide 12	6.57
	Cyp2d9	cytochrome P450, family 2, subfamily d, polypeptide 9	8.56

Cyp2f2	cytochrome P450, family 2, subfamily f, polypeptide 2	3.29
Cyp2j9	cytochrome P450, family 2, subfamily j, polypeptide 9	2.16
Cyp3a11	cytochrome P450, family 3, subfamily a, polypeptide 11	3.94
Cyp4a32	cytochrome P450, family 4, subfamily a, polypeptide 32	2.03
Cyp4v3	cytochrome P450, family 4, subfamily v, polypeptide 3	2.60
Ero1lb	ERO1-like beta (S. cerevisiae)	2.65
Fmo5	flavin containing monooxygenase 5	2.74
Nox4	NADPH oxidase 4	3.78
Akr1b7	aldo-keto reductase family 1, member B7	−3.29
Cyb561	cytochrome b-561	−2.30
Cyp17a1	cytochrome P450, family 17, subfamily a, polypeptide 1	−3.27
Cyp2c37	cytochrome P450, family 2. subfamily c, polypeptide 37	−2.35
Cyp2c39	cytochrome P450, family 2, subfamily c, polypeptide 39	−3.08
Cyp51	cytochrome P450, family 51	−2.45
Fmo3	flavin containing monooxygenase 3	−12.58
Rdh11	retinol dehydrogenase 11	−2.03
Rdh9	retinol dehydrogenase 9	−2.65
Mgst3	microsomal glutathione S-transferase 3	−2.40
Nqo1	NAD(P)H dehydrogenase, quinone 1	−2.19
S100a9	S100 calcium binding protein A9 (calgranulin B)	−5.95

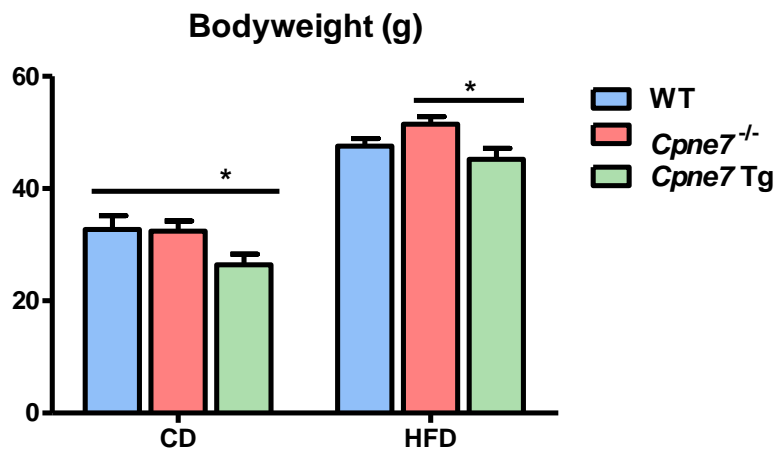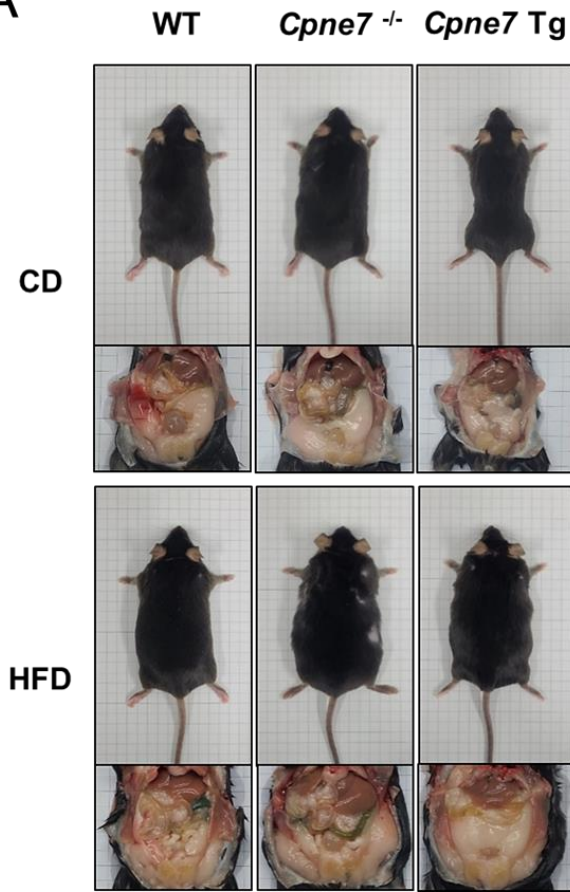### 3.3. *Cpne7* is associated with whole-body lipid metabolism.

To further investigate the role of *Cpne7* in whole-body lipid metabolism *in vivo*, we established a HFD-induced mouse model. HFD feeding was performed in WT, *Cpne7*$^{-/-}$, and *Cpne7* Tg mice for 16 weeks (n = 6). During macroscopic analyses, HFD-fed mice showed increased body sizes, amounts of visceral fat and bodyweights compared with CD-fed mice. In CD-fed mice, body sizes, visceral fat amounts and bodyweights of *Cpne7* Tg mice were markedly decreased compared to those of WT mice. In HFD-fed mice, body sizes and visceral fat amounts of *Cpne7*$^{-/-}$ mice were noticeably increased compared to those of WT mice. The bodyweights of HFD-fed *Cpne7* Tg mice were significantly reduced compared to those of *Cpne7*$^{-/-}$ mice (Figure 7A).

Subsequently, DXA was used to measure the body fat, bone mineral, lean content of each group. The images of each group were presented as radiographs of the body composition. The average of the measured percentages and mass of fat, bone mineral and lean were expressed as a graph. In CD-fed mice, the fat percentage of *Cpne7* Tg mice was significantly reduced compared to those of WT and *Cpne7*$^{-/-}$ mice. In HFD-fed mice, the fat percentage was significantly increased in *Cpne7*$^{-/-}$ mice compared to WT mice. The percentages of bone mineral and lean were opposite to that of fat (Figure 7B).

Blood tests in each group were performed after overnight fasting. Regarding the levels of liver damage markers, no difference in albumin was found. In HFD-fed mice, the ALT levels of *Cpne7*$^{-/-}$

mice were significantly increased compared to those of WT mice. ALT levels of HFD-fed *Cpne7* Tg mice were significantly decreased compared to those of HFD-fed *Cpne7*$^{-/-}$ mice; however, the levels were still higher than those of WT mice. Subsequently, T. chol levels were considerably decreased in *Cpne7* Tg mice compared with *Cpne7*$^{-/-}$ among HFD-fed mice. TG levels were significantly decreased in *Cpne7* Tg mice compared with both WT and *Cpne7*$^{-/-}$ among HFD-fed mice. FFA levels of CD-fed *Cpne7* Tg mice were decreased compared to those of CD-fed *Cpne7*$^{-/-}$ mice. Furthermore, glucose levels were significantly increased in CD- and HFD-fed *Cpne7*$^{-/-}$ mice compared to WT mice, and were decreased in CD-fed *Cpne7* Tg mice compared to CD-fed *Cpne7*$^{-/-}$ mice (Figure 7C). These results shows that *Cpne7* deficiency induced abnormal lipid metabolism, resulting in changed serum levels of ALT and lipid-related markers.

A

Bodyweight (g)

B

| | WT | Cpne7 $^{-/-}$ | Cpne7 Tg |

CD

HFD

Fat percentage (%)

Fat mass (g)

Bone mineral contents (%)

Bone mineral contents (g)

Lean percentage (%)

Lean mass (g)

C

Albumin (g/dL)

WT
Cpne7^{-/-}
Cpne7 Tg

ALT (U/L)

***
***
**

WT
Cpne7^{-/-}
Cpne7 Tg

T.chol (mg/dL)

**

WT
Cpne7^{-/-}
Cpne7 Tg

cTG (mg/dL)

**
*

WT
Cpne7^{-/-}
Cpne7 Tg

FFA (µ Eq/L)

*

WT
Cpne7^{-/-}
Cpne7 Tg

Glucose (mg/dL)

**
*
**

WT
Cpne7^{-/-}
Cpne7 Tg

7 2
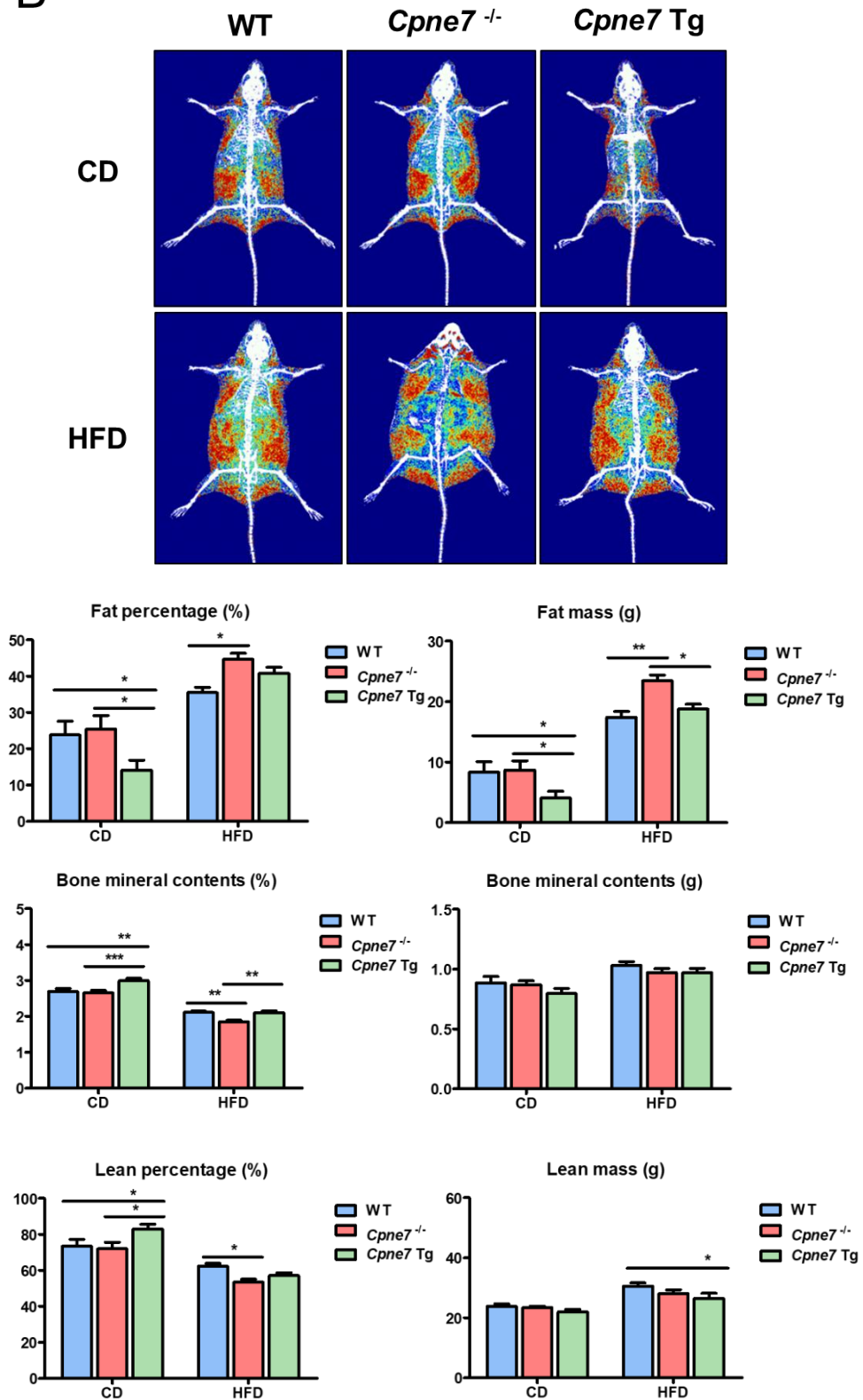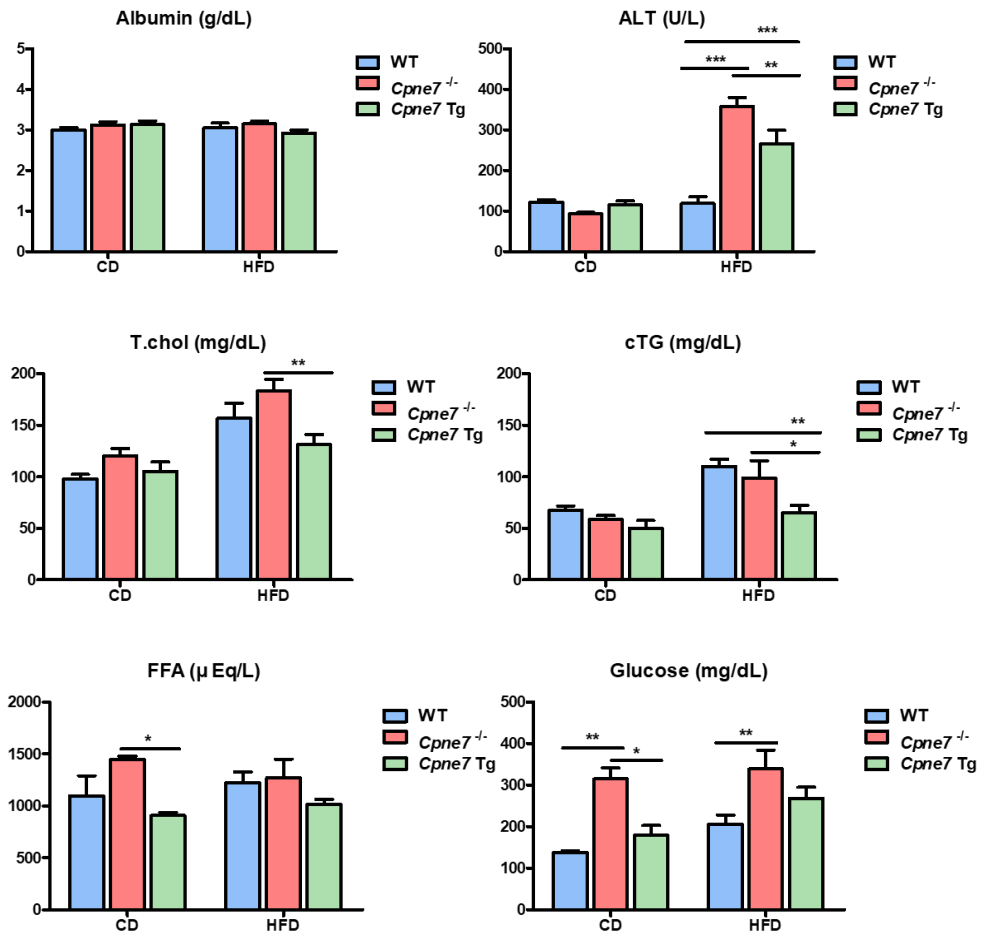
Figure 7. *Cpne7* is related to whole-body lipid metabolism. (A) Representative macroscopic images of body and visceral fat, and bodyweights in chow diet (CD)-fed and high fat diet (HFD)-fed WT, *Cpne7*$^{-/-}$ and *Cpne7*-overexpressing transgenic (*Cpne7* Tg) mice. (B) Representative images of body composition (red = fat tissue, blue = lean tissue), and quantitative analysis of fat, bone mineral, lean contents in CD-fed and HFD-fed WT, *Cpne7*$^{-/-}$ and *Cpne7* Tg mice. (C) Serum levels of albumin, alanine aminotransferase (ALT), total cholesterol (T.chol), triglyceride (TG), free fatty acid (FFA), and glucose in CD-fed and HFD-fed WT, *Cpne7*$^{-/-}$ and *Cpne7* Tg mice. (*p< 0.05, **p <0.01 and ***p <0.001)

3.4. *Cpne7* deficiency promotes severe hepatic steatosis in the HFD-induced NAFLD model

To examine the effect of *Cpne7* on the hepatic lipid metabolism, macroscopic and histological analyses were performed. In the HFD-induced NAFLD model, macroscopic analyses demonstrated that the livers of *Cpne7*$^{-/-}$ mice were larger and had more pale-yellow appearances than those of WT mice. Moreover, liver weights of HFD-fed mice were significantly increased in *Cpne7*$^{-/-}$ mice compared to WT mice and markedly decreased in *Cpne7* Tg mice compared to *Cpne7*$^{-/-}$ mice (Figure 8A).

During histological analyses, several LDs were observed in the livers of *Cpne7*$^{-/-}$ mice even among CD-fed mice. The livers of HFD-fed *Cpne7*$^{-/-}$ mice showed severe steatosis features such as excessive lipid accumulation and hepatocyte ballooning. According to LD quantification in the H&E-stained images, in HFD-fed mice, the percentage of steatosis were significantly higher in *Cpne7*$^{-/-}$ mice than in WT mice and were significantly lower in *Cpne7* Tg mice than *Cpne7*$^{-/-}$ mice; although, the levels of *Cpne7* Tg mice were still higher than those of WT mice (Figure 8B). These results suggest that *Cpne7* deficiency accelerates hepatic lipid accumulation in the HFD-induced NAFLD model.

A

	WT	Cpne7 $^{-/-}$	Cpne7 Tg

CD

HFD

Liver weight (g)

- WT
- *Cpne7* $^{-/-}$
- *Cpne7* Tg

B

Steatosis (%)
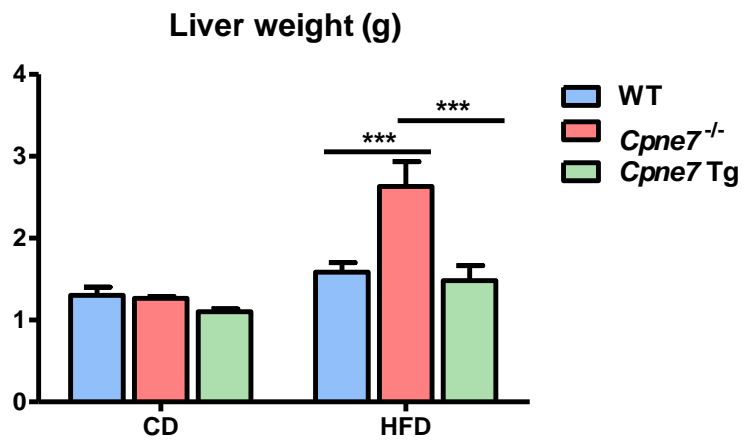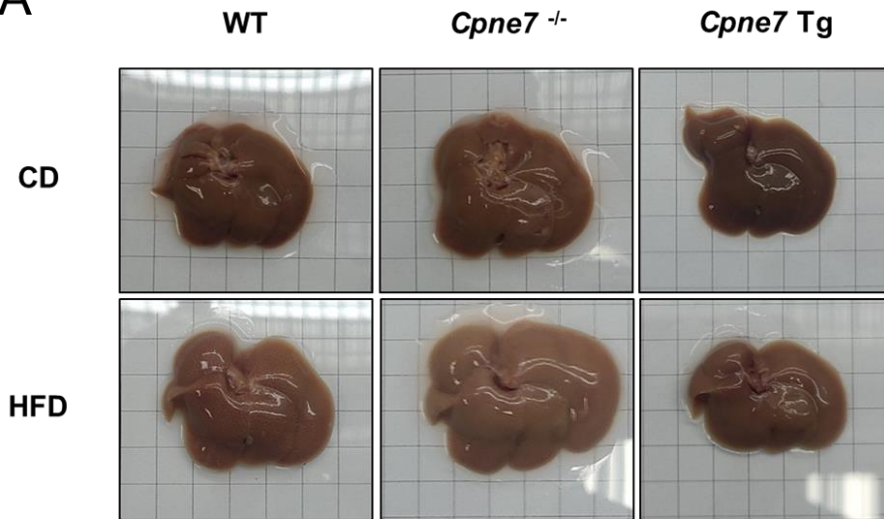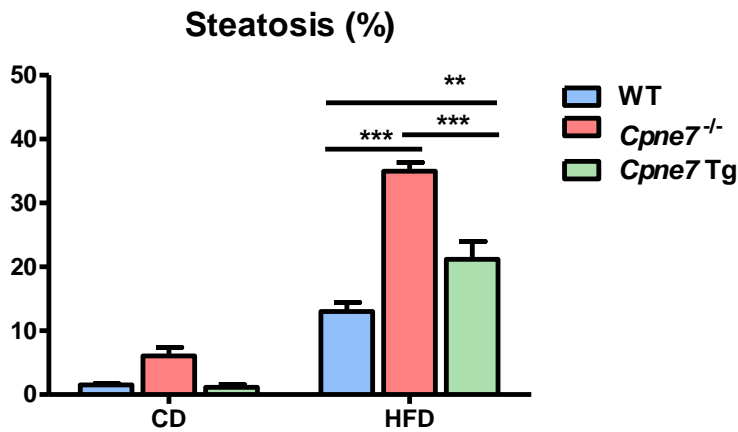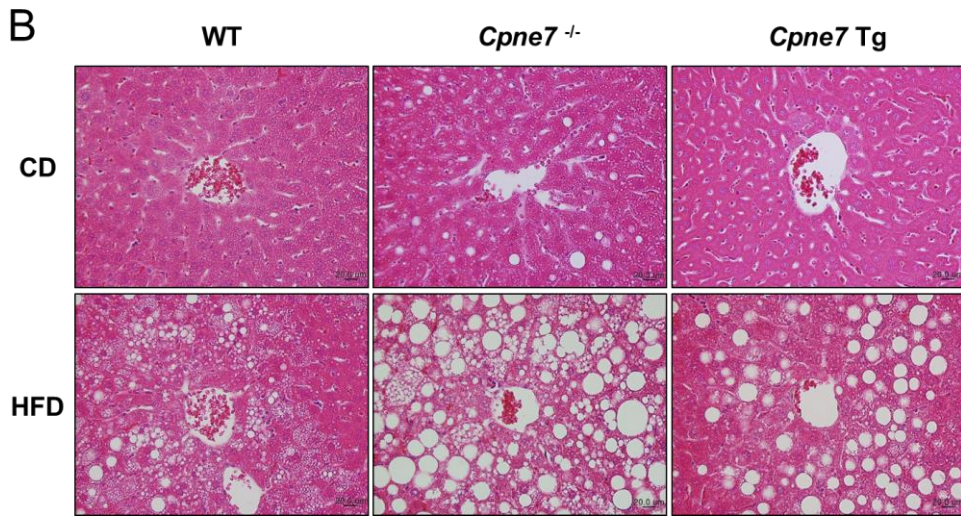
Figure 8. *Cpne7* deficiency accelerates hepatic fatty changes in the HFD-induced NAFLD model. (A) Representative macroscopic liver images and liver weights in CD-fed and HFD-fed WT, *Cpne7*^{-/-} and *Cpne7* Tg mice (B) H&E-stained images in the livers of CD-fed and HFD-fed WT, *Cpne7*^{-/-} and *Cpne7* Tg mice (scale bars = 20 μm), and quantitative analysis of percentage of steatosis using Image J software. (*p< 0.05, **p <0.01 and ***p <0.001)

3.5. *Cpne7* deficiency leads to mitochondrial dysfunction in the livers

To identify how *Cpne7* deficiency induced lipid accumulation, we analyzed mitochondrial function, which is known to be strongly associated with lipid metabolism (Koliaki et al. 2015; Moore et al. 2022; Peng et al. 2018; Rolo et al. 2012). A TEM analysis was performed to compare the mitochondrial morphology. In CD-fed mice, the hepatic mitochondria of $Cpne7^{-/-}$ mice were swollen and lost cristae; however, those of WT and *Cpne7* Tg mice did not (Figure 9A). The hepatic mitochondria of HFD-fed WT and *Cpne7* Tg mice were swollen, and cristae loss was observed compared to those of CD-fed mice. The most striking result to emerge from TEM data is that most mitochondria were destroyed, and abnormal mitochondrial morphologies were observed due to severe cell damage in the livers of HFD-fed $Cpne7^{-/-}$ mice (Figure 9B).

In the marker expression analysis of mitochondrial dynamics, fission regulators such as the mitochondrial fission factor (MFF) and mitochondrial fission protein 1 (FIS1) were significantly increased in the livers of CD-fed *Cpne7* Tg mice. In HFD-fed mice, fission regulators such as dynamin-related protein 1 (DRP1), MFF, and FIS1 and fusion regulators such as mitofusin 1 and 2 (MFN 1, 2) were significantly decreased in the livers of $Cpne7^{-/-}$ mice compared to those of WT mice. These fission regulators were significantly increased in the livers of *Cpne7* Tg mice compared to those of $Cpne7^{-/-}$ mice. (Figure 9C). These findings suggest that *Cpne7* deficiency results in hepatic mitochondrial damages such as

abnormal morphology and decreased mitochondrial dynamics.

A

CD - WT

CD - *Cpne7* -/-

CD - *Cpne7* Tg

B

HFD - WT

HFD - *Cpne7* -/-

HFD - *Cpne7* Tg

C

CD

HFD

WT   Cpne7 -/-   Cpne7 Tg   WT   Cpne7 -/-   Cpne7 Tg

1 2 3 4   1 2 3 4   1 2 3 4   1 2 3 4   1 2 3 4   1 2 3 4

DRP1
MFF
FIS1
MFN1
MFN2
CPNE7
GAPDH

Legend (top graph):
- CD - WT
- CD - Cpne7 -/-
- CD - Cpne7 Tg

Y-axis: Relative protein expression [Protein/GAPDH]

X-axis categories: DRP1 MFF FIS1 MFN1 MFN2 CPNE7

Legend (bottom graph):
- HFD - WT
- HFD - Cpne7 -/-
- HFD - Cpne7 Tg

Y-axis: Relative protein expression [Protein/GAPDH]

X-axis categories: DRP1 MFF FIS1 MFN1 MFN2 CPNE7

7 9

Figure 9. *Cpne7* deficiency induces mitochondrial ultrastructural abnormalities and changes of mitochondrial dynamics. (A) TEM images in the livers of CD-fed WT, *Cpne7*$^{-/-}$ and *Cpne7* Tg mice. The right column (scale bars = 1 μm) was investigated under magnification of the left column (boxed area, scale bars = 500 nm). (B) TEM images in the livers of HFD-fed WT, *Cpne7*$^{-/-}$ and *Cpne7* Tg mice. The right column (scale bars = 1 μm) was investigated under magnification of the left column (boxed area, scale bars = 500 nm). (C) Western blot analysis of mitochondrial fission and fusion protein levels in the livers of CD-fed and HFD-fed WT, *Cpne7*$^{-/-}$ and *Cpne7* Tg mice, and quantification of mitochondrial fission and fusion protein levels. (*p< 0.05, **p <0.01 and ***p <0.001)

3.6. *Cpne7* deficiency causes mitochondrial dysfunction-induced ROS overproduction, resulting in hepatic lipid accumulation *in vivo* and *in vitro*

To assess whether *Cpne7* deficiency-induced mitochondrial dysfunction could elicit excessive ROS production, we measured the ROS levels. High ROS production was observed in the livers of CD-fed and HFD-fed *Cpne7*$^{-/-}$ mice. The ROS levels in the livers of CD-fed *Cpne7* Tg mice were significantly decreased compared with those in the livers of CD-fed *Cpne7*$^{-/-}$ mice; however, the levels did not differ significantly in the livers of HFD-fed *Cpne7* Tg mice (Figure 10).

To validate the role of *CPNE7* on ROS levels, mitochondrial dysfunction and lipid metabolism in hepatocytes *in vitro*, HepG2 cells were transfected with shRNA and expression vectors of *CPNE7*. The transfection efficiency was evaluated via protein levels of CPNE7. Compared with controls, protein levels of CPNE7 were significantly decreased and increased by sh*CPNE7* and *CPNE7* overexpression (o/e), respectively (Figure 11A). In H_2O_2-induced oxidative stress, cellular ROS was increased in *CPNE7*-silenced cells compared with controls, and *CPNE7*-overexpressed cells showed decreased ROS levels compared with *CPNE7*-silenced cells (Figure 11B). Mitochondrial respiration in H_2O_2-treated HepG2 cells was significantly decreased compared to HepG2 cells not treated with H_2O_2. In H_2O_2-induced oxidative stress, maximal respiration is significantly reduced in *CPNE7*-silenced cells compared with controls, *CPNE7*-overexpressed cells showed

increased mitochondrial function including basal respiration, ATP production, and maximal respiration (Figure 11C). In the results of oil-red O staining, *CPNE7*-silenced cells showed markedly increased lipid contents, and lipid contents in *CPNE7*-overexpressed cells were significantly decreased compared with those of controls under H_2O_2-induced oxidative stress (Figure 11D). These results implicate that *CPNE7* deficiency promotes hepatic lipid accumulation by causing excessive ROS production due to mitochondrial dysfunction.

A

| ROS | DAPI | T-PMT | Merged |

CD - WT

CD - *Cpne7* -/-

CD - *Cpne7* Tg

B

| ROS | DAPI | T-PMT | Merged |

HFD - WT

HFD - *Cpne7* -/-
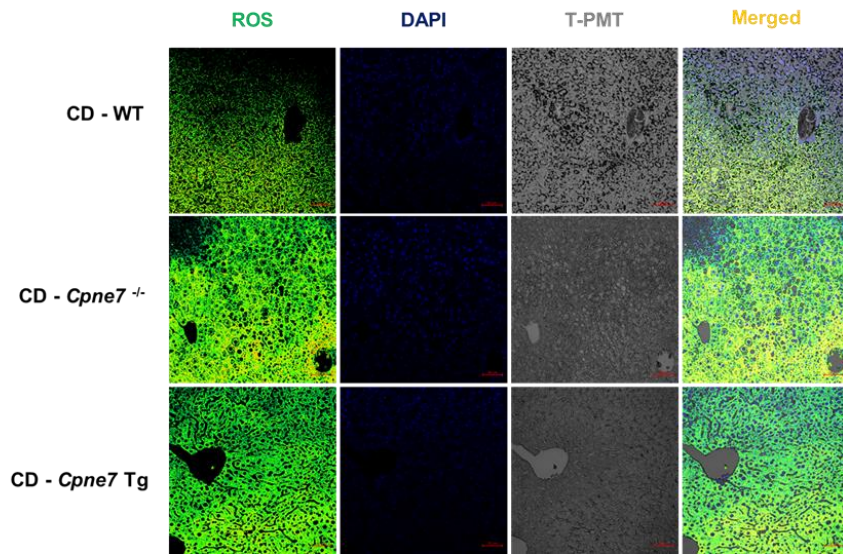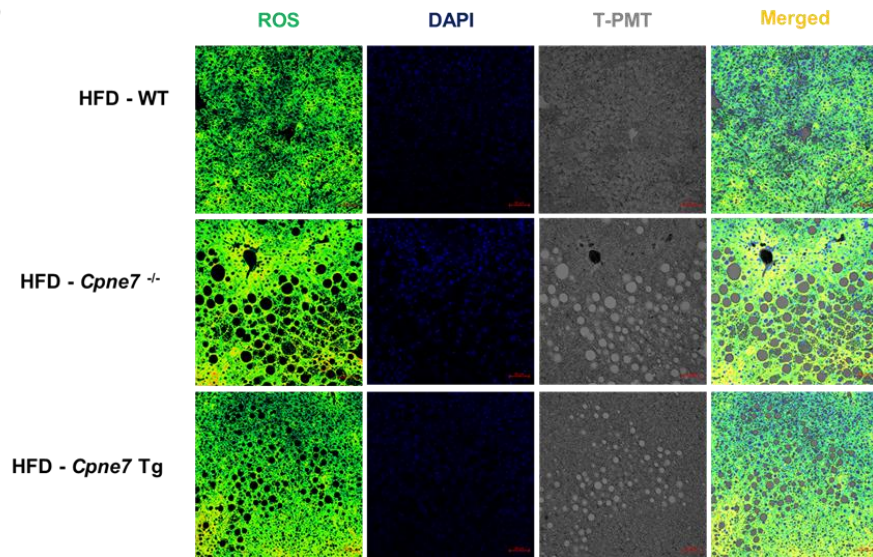
HFD - *Cpne7* Tg

C
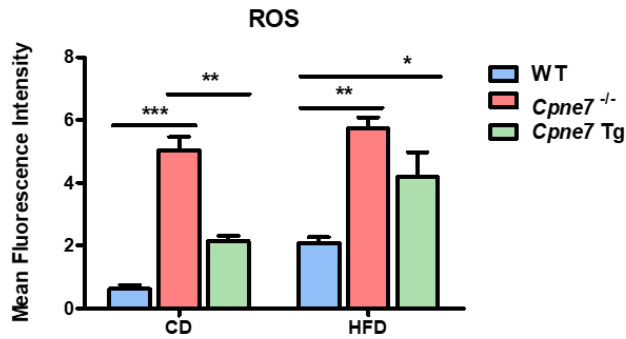
Figure 10. *Cpne7* deficiency increases hepatic ROS levels in both CD-fed and HFD-fed mice. (A) Representative fluorescence images of DCFDA for ROS detection in the livers of CD-fed WT, *Cpne7*$^{-/-}$ and *Cpne7* Tg mice. Images were used of pseudo-color look-up table (LUT). The LUT setting were assigned for pixels with blue of low intensity, yellow of intermediate intensity and red of high intensity (scale bars = 50 μm). (B) Representative fluorescence images of DCFDA for ROS detection in the livers of HFD-fed WT, *Cpne7*$^{-/-}$ and *Cpne7* Tg mice (scale bars = 50 μm). (C) Quantification of ROS levels. (*p< 0.05, **p <0.01 and ***p <0.001)

A

CPNE7 — 60

GAPDH — 35

B

Cellular ROS

C

Mitochondrial Respiration

D

	Control	shCPNE7	CPNE7 o/e

Control

H_2O_2 (200μm, 24h)

Lipid content
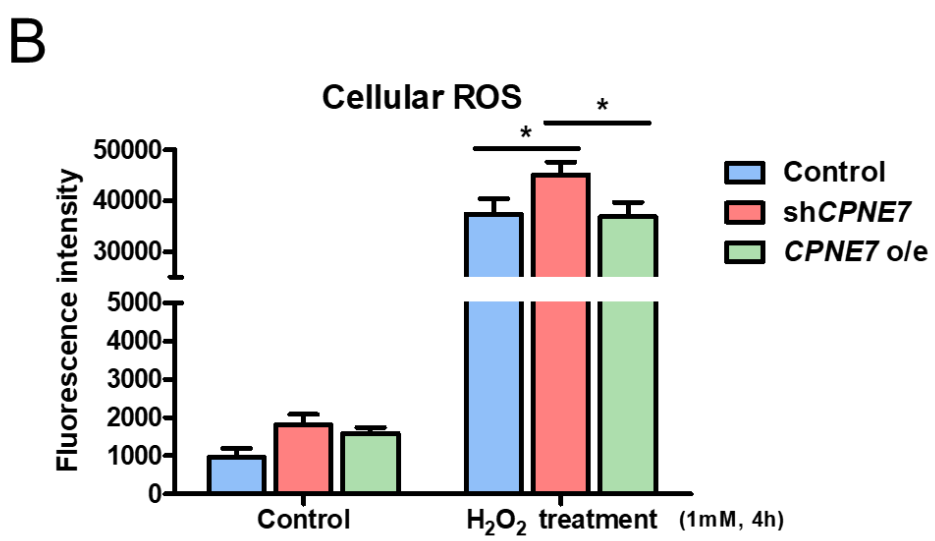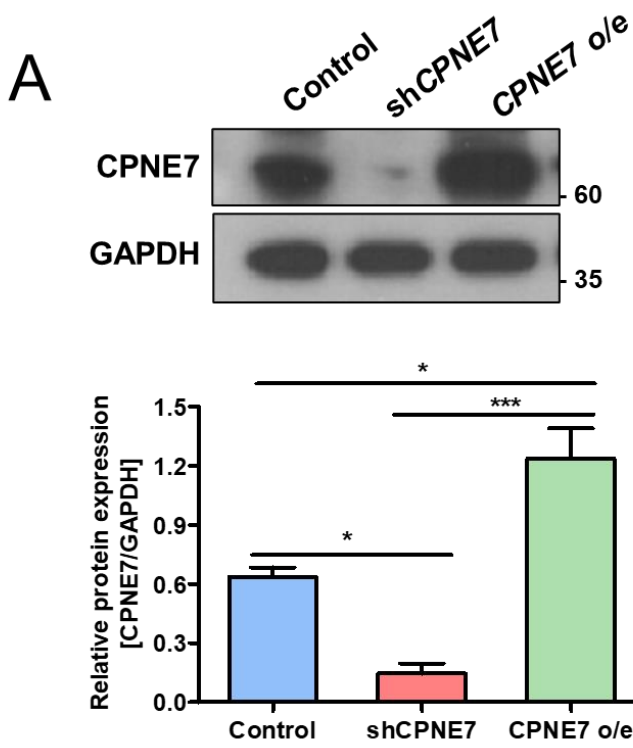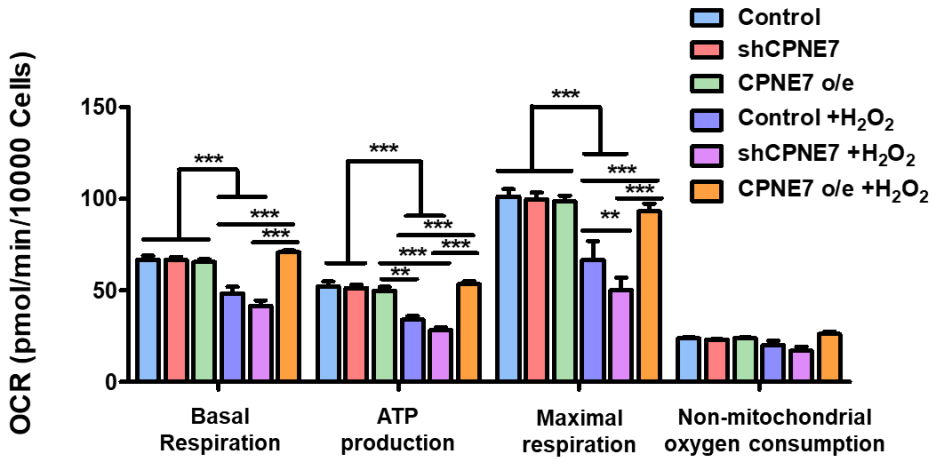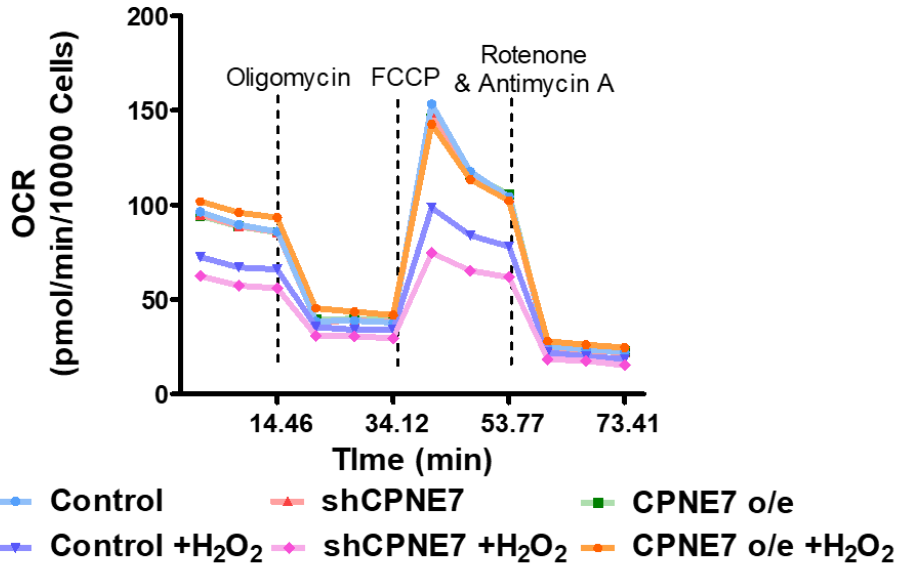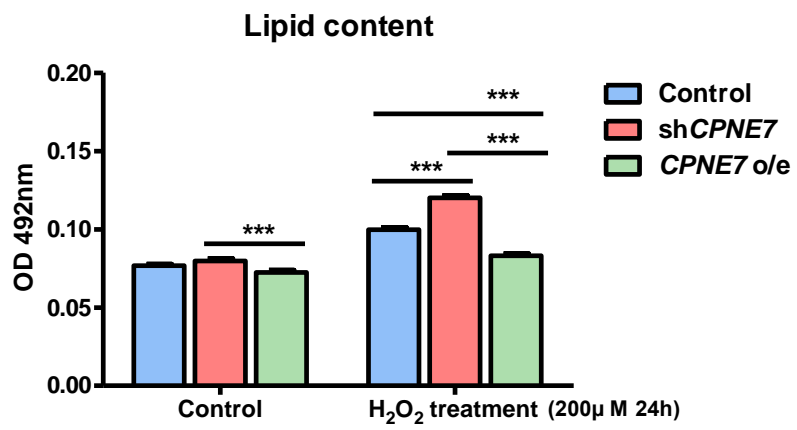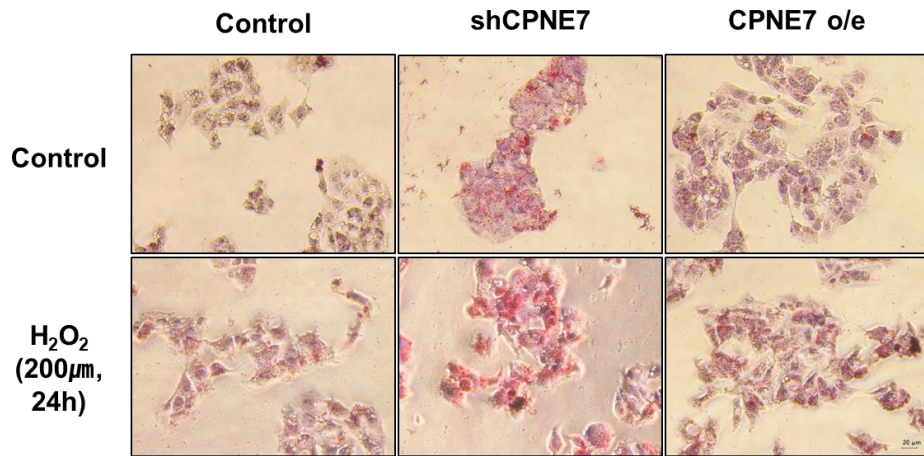
Figure 11. *CPNE7* silencing causes mitochondrial dysfunction and lipid accumulation with high ROS level in H_2O_2-induced HepG2 cells. (A) CPNE7 expression by western blotting to assess the efficiency of sh*CPNE7*, and *CPNE7* overexpression vector (o/e) transfection in HepG2 cells. (B) Fluorescence intensity of cellular ROS in control, sh*CPNE7*, and *CPNE7* o/e transfected HepG2 cells with control and H_2O_2-induced oxidative stress. (C) Representative and statistical results of mitochondrial respiration in control, shCPNE7, and CPNE7 o/e transfected HepG2 cells with control and H_2O_2-induced oxidative stress (D) Oil-red O staining for detection of lipid content in control, sh*CPNE7*, and *CPNE7* o/e transfected HepG2 cells with control and H_2O_2-induced oxidative stress (scale bars = 20 μm) and quantification of oil-red O analysis. (*p< 0.05, **p <0.01 and ***p <0.001)

4. Discussion

Previous studies have emphasized that hepatic mitochondria play a role in the pathogenesis of NAFLD (Begriche et al. 2006; Pessayre and Fromenty 2005; Pessayre et al. 2002). Mitochondrial dysfunction increases ROS production and affects hepatic lipid homeostasis. Excessive ROS formation exceeding the antioxidant capacity causes cell injury and oxidative stress (Begriche et al. 2006). Moreover, excessive ROS production induces the accumulation of intracellular LDs and disrupts lipid homeostasis, contributing to the development and progression of NAFLD (Jin et al. 2018; Mansouri et al. 2018).

In this study, we investigated whether *Cpne7* affects hepatic lipid metabolism and mitochondrial function using *Cpne7* mutant mice *in vivo* and *Cpne7*-silenced and *Cpne7*-overexpressed HepG2 cells *in vitro*. The DEGs in the livers of *Cpne7*$^{-/-}$ mice were involved in lipogenesis and mitochondrial dysfunction. *Srebf1*, a transcription factor for lipogenesis (Horton et al. 2002), was increased, and most of its downstream lipogenic genes were significantly increased. Fatty acid synthesis genes were significantly upregulated. In addition, hormone-related genes, such as *Lepr* and *Igfbp1*, were downregulated, linking that not only fat accumulation but also insulin resistance (Mammes et al. 2001; Rajwani et al. 2012). In DEGs with oxidoreductase activity, changes in the *Cyps* expression were noticeable. Considering that *Cyps* are

expressed in mitochondria and plays roles in xenobiotics and steroid hormone metabolism (Bibi 2008; Knockaert et al. 2011; Zhang and Yang 2009), changes of these gene expression could be related to mitochondrial function, hepatotoxicity, and insulin resistance. Furthermore, *Cyps* and *Nox4* are known the sources of ROS (Hrycay and Bandiera 2015; Weyemi and Dupuy 2012). In contrast, there was a downregulation of genes involved in antioxidant activity. These findings suggest that *Cpne7* deficiency could cause lipogenesis, elevated ROS levels, and mitochondrial dysfunction.

Indeed, typical pathological manifestations of NAFLD, such as increased liver sizes, pale-yellow appearances, severe steatosis, and hepatocyte ballooning, were accelerated in the livers of HFD-fed *Cpne7*$^{-/-}$ mice compared with those of HFD-fed WT mice. Additionally, numerous LDs were observed in the livers of CD-fed *Cpne7*$^{-/-}$ mice but not in those of CD-fed WT and *Cpne7* Tg mice. Interestingly, *Cpne7* deficiency not only resulted in fatty changes in the liver but also mitochondrial dysfunction. Abnormal mitochondrial morphology and high ROS levels were observed in CD-fed and HFD-fed *Cpne7*$^{-/-}$ mice. Furthermore, In line with the results of *in vivo* investigations, high ROS levels, mitochondrial dysfunction and lipid accumulation were observed in H_2O_2-induced sh*CPNE7* HepG2 cells.

These results align with several previous studies indicating that mitochondrial ultrastructural abnormalities appeared with increasing NAFLD severity (Caldwell et al. 2009; Caldwell et al. 1999; Pirola

et al. 2013; Sanyal et al. 2001). The deterioration of the mitochondrial morphology may indicate an increase in oxidative stress and the disruption of the biological system regulating mitochondrial biogenesis, mitophagy, fission and fusion (Moore et al. 2022). Several reports have shown that DRP1, a key regulator of mitochondrial fission, was reduced in a rodent model of western diet-induced NASH and liver-specific deletion of DRP1 caused the loss of fatty acid oxidation (Krishnasamy et al. 2019; Yamada et al. 2018). Consistent with the findings of previous studies, mitochondrial fission regulators such as DRP1, MFF, and FIS1 in the livers of HFD-fed $Cpne7^{-/-}$ mice were significantly reduced compared to those of HFD-fed WT mice. This inhibition of mitochondrial fission could induce the accumulation of damaged mitochondria, which could exacerbate mitochondrial dysfunction (Twig et al. 2008; Twig and Shirihai 2011). Recently, Mary P. Moore et al. reported that the levels of markers of mitochondrial turnover decreased with the severity of human NAFLD and that low levels of these markers could trigger mitochondrial dysfunction and progression to NASH (Moore et al. 2022). Based on the findings of these studies, we suggest that $Cpne7$ deficiency causes mitochondrial dysfunction, exacerbating hepatic lipid metabolism.

However, there are some unanswered questions. In injury models such as HFD-fed $Cpne7^{-/-}$ mice or H_2O_2-treated sh$CPNE7$ HepG2 cells, lipogenesis was noticeably increased and mitochondrial function was significantly reduced. This tendency was similar not only in hepatocytes but also in odontoblasts and PDL

fibroblasts. A similar pattern was also seen in the brain; *Cpne7*-knockout(KO) increased the amount of REM sleep in cage-changing or water immersion and restraint stress (WIPS) environments, whereas normal sleep was observed under basal conditions(Liu et al. 2021). Therefore, the actions of CPNE7 appear to be more noticeable in response to environmental stimuli or stressful environments than in the basal condition. Although the mechanism is still unclear, it is speculated that CPNE7 is related to the homeostatic effect and further research is required. Additionally, further measurements of hepatic cholesterol and TG levels are needed since neither serum cholesterol nor cTG levels in HFD-fed *Cpne7*$^{-/-}$ mice were significantly elevated. HFD feeding in this study performed on young mice (6-week-old). Considering that metabolic diseases are closely involved in aging, further studies on the effect of CPNE7 are needed in HFD-fed old mice (18-month-old).

Furthermore, the discrepancy of the liver phenotype was observed according to the diet in *Cpne7* Tg mice. CD-fed *Cpne7* Tg mice had significantly decreased bodyweights and fat percentages compared with CD-fed WT mice. Moreover, fewer LDs and normal mitochondrial morphologies were observed, and ROS levels did not differ significantly in the livers of CD-fed *Cpne7* Tg mice compared to those of CD-fed WT mice. On the other hand, in HFD-fed *Cpne7* Tg mice, although the serum cTG levels were significantly decreased compared with HFD-fed WT mice, larger LDs and higher ROS levels were observed than in HFD-fed WT mice. It is difficult

to explain these results; however, a possible explanation for this might be as a result of the use of HFD-fed animal model. In general, HFD has been linked to a number of negative outcomes, including obesity, insulin resistance, altered microbiota, and inflammatory response (Maharjan et al. 2021; Murphy et al. 2015). Under the circumstances where HFD-induced multiple responses are complicatedly intertwined, there could be a portion where *Cpne7* does not function. As there are numerous potential factors and clear mechanisms have not yet been established, further investigations are required, including utilizing additional animal models. Indeed, in H_2O_2-induced oxidative stress *in vitro* model, not the HFD, mitochondrial function was significantly enhanced and the lipid content was significantly reduced in *CPNE7*-overexpressed HepG2 cells compared to controls. Additionally, in both CD-fed and HFD-fed *Cpne7* Tg mice, the levels of MFF and FIS1 increased noticeably. Furthermore, a recent study demonstrated that increased hepatic FIS1 modulates the mitochondrial integrated stress response and restores metabolic homeostasis (Liou et al. 2022). These findings suggest that *Cpne7* overexpression may alleviate aberrant lipid metabolism by modulating the mitochondrial function. Still, further research is required to understand the relationship between *Cpne7* overexpression and NAFLD and to explore the mechanisms of action of *Cpne7* in NAFLD.

Previous studies suggest that NAFLD might be a mitochondrial disease (Nassir and Ibdah 2014). This study shows that *Cpne7* deficiency deteriorates hepatic lipid metabolism by mitochondrial

dysfunction−induced excessive ROS production. In conclusion, this study highlights the critical role of *CPNE7* in hepatic mitochondrial function and the development of NAFLD, suggesting *Cpne7* as a novel therapeutic target for NAFLD. The insights gained from this study contribute to the understanding of the pathogenesis of NAFLD.

Chapter Ⅲ. Concluding Remarks

The present dissertation, which was separated into parts 1 and 2, attempted to evaluate the mitochondria-based roles and effects of CPNE7 in odontoblasts and hepatocytes.

In part 1, the oral cavity is a place where ROS can rapidly build up due to exposure to numerous stimuli. The control of ROS levels is directly tied to mitochondrial function. Odontoblasts are long-lived post-mitotic cells; mature odontoblasts exhibit age-related increase of ROS and mitochondrial dysfunction. This research demonstrates that CPNE7-DP significantly enhanced mitochondrial function in H_2O_2-treated hDPCs, implicating that CPNE7-DP plays a role in mitochondrial function in hDPCs. In addition, tertiary dentin formation and dentin sealing effects were evaluated using CPNE7-DP-containing toothpaste and two commercially available toothpastes. The evaluations revealed that CPNE7-DP-containing toothpaste can induce tertiary dentin formation to promote a sustained dentin sealing effect and act as a successful desensitizer. Overall, this study suggests the possibility that CPNE7-DP can enhance mitochondrial function, resulting in tertiary dentin formation and dentin sealing effect under oxidative stress.

In part 2, hepatic mitochondria play an important role in the development of NAFLD. Mitochondrial dysfunction causes excessive ROS production, resulting in deterioration of lipid metabolism. Cell injury and oxidative stress are consequences of

excessive ROS production. In addition, increased ROS production promotes the accumulation of intracellular lipid droplets and interferes with lipid homeostasis, which contributes to the development and progression of NAFLD. In this study, RNA-sequencing analysis showed that *Cpne7* deficiency is involved in hepatic lipid and redox metabolism. *Cpne7* deficiency caused high ROS levels and abnormal mitochondrial morphology in the livers. In the HFD-induced NAFLD model, severe hepatic steatosis and defected mitochondrial dynamics was promoted by *Cpne7* deficiency. These results suggest that *Cpne7* deficiency induces excessive ROS production and mitochondrial dysfunction, which promotes disrupted lipid metabolism.

Altogether, CPNE7 affects the mitochondrial function of odontoblasts and hepatocytes. These effects appear in the regulation of dentin formation and lipid metabolism, which are the intrinsic functions of each cell.

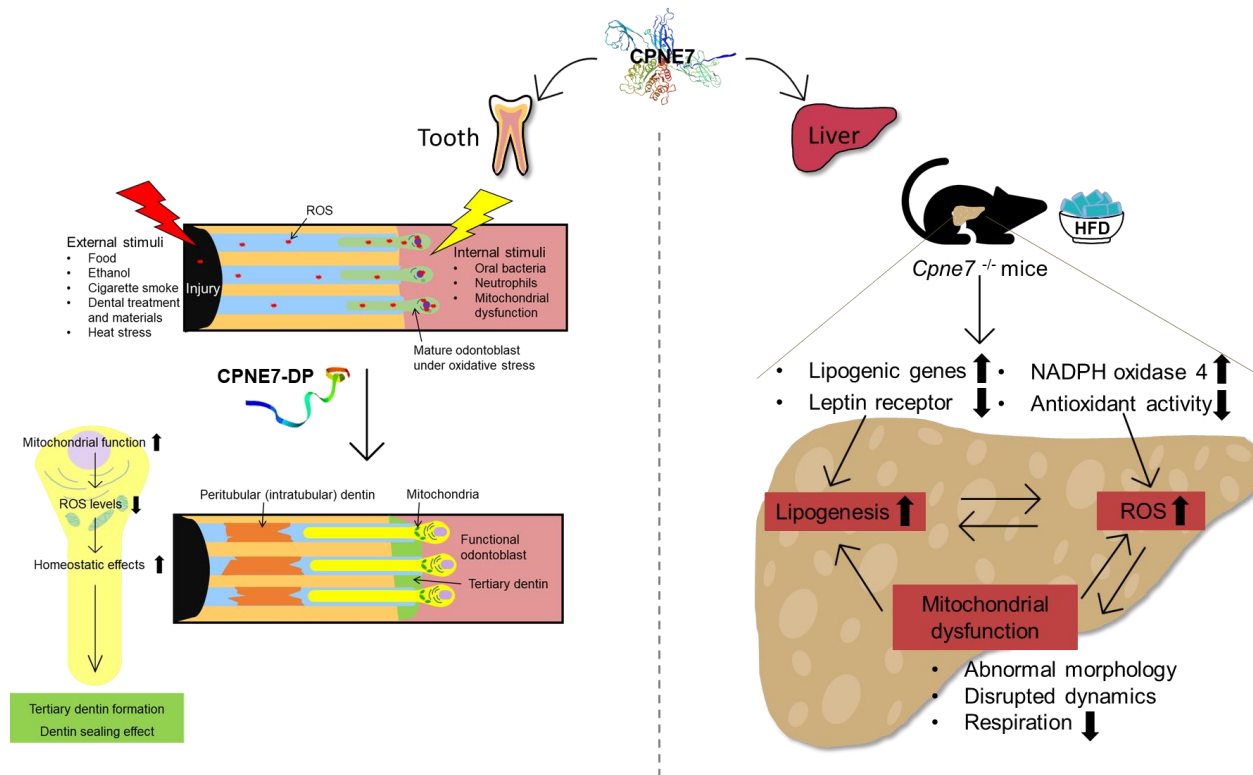Figure 12. Schematic illustration of effects of CPNE7 on odontoblasts and hepatocytes based on mitochondrial function. CPNE7-DP can enhance mitochondrial function of odontoblasts, leading to tertiary dentin formation and dentin sealing effect under oxidative stress. In the liver, *Cpne7* deficiency causes excessive ROS formation and mitochondrial dysfunction, which aggravates lipid metabolism abnormalities

References

Addy M, West NX. 2013. The role of toothpaste in the aetiology and treatment of dentine hypersensitivity. Monogr Oral Sci. 23:75-87.

Arnold WH, Groger C, Bizhang M, Naumova EA. 2016. Dentin abrasivity of various desensitizing toothpastes. Head Face Med. 12:16.

Arnold WH, Prange M, Naumova EA. 2015. Effectiveness of various toothpastes on dentine tubule occlusion. J Dent. 43(4):440-449.

Barja G. 2013. Updating the mitochondrial free radical theory of aging: An integrated view, key aspects, and confounding concepts. Antioxid Redox Signal. 19(12):1420-1445.

Begriche K, Igoudjil A, Pessayre D, Fromenty B. 2006. Mitochondrial dysfunction in nash: Causes, consequences and possible means to prevent it. Mitochondrion. 6(1):1-28.

Bibi Z. 2008. Role of cytochrome p450 in drug interactions. Nutr Metab (Lond). 5:27.

Brand MD, Affourtit C, Esteves TC, Green K, Lambert AJ, Miwa S, Pakay JL, Parker N. 2004. Mitochondrial superoxide: Production, biological effects, and activation of uncoupling proteins. Free Radic Biol Med. 37(6):755-767.

Brannstrom M. 1986. The hydrodynamic theory of dentinal pain: Sensation in preparations, caries, and the dentinal crack

syndrome. J Endod. 12(10):453-457.

Brookes PS, Yoon Y, Robotham JL, Anders MW, Sheu SS. 2004. Calcium, atp, and ros: A mitochondrial love-hate triangle. Am J Physiol Cell Physiol. 287(4):C817-833.

Bugianesi E, Moscatiello S, Ciaravella MF, Marchesini G. 2010. Insulin resistance in nonalcoholic fatty liver disease. Curr Pharm Des. 16(17):1941-1951.

Buzzetti E, Pinzani M, Tsochatzis EA. 2016. The multiple-hit pathogenesis of non-alcoholic fatty liver disease (nafld). Metabolism. 65(8):1038-1048.

Byrne CD, Targher G. 2015. Nafld: A multisystem disease. J Hepatol. 62(1 Suppl):S47-64.

Caldwell SH, de Freitas LA, Park SH, Moreno ML, Redick JA, Davis CA, Sisson BJ, Patrie JT, Cotrim H, Argo CK et al. 2009. Intramitochondrial crystalline inclusions in nonalcoholic steatohepatitis. Hepatology. 49(6):1888-1895.

Caldwell SH, Swerdlow RH, Khan EM, Iezzoni JC, Hespenheide EE, Parks JK, Parker WD, Jr. 1999. Mitochondrial abnormalities in non-alcoholic steatohepatitis. J Hepatol. 31(3):430-434.

Chalasani N, Younossi Z, Lavine JE, Charlton M, Cusi K, Rinella M, Harrison SA, Brunt EM, Sanyal AJ. 2018. The diagnosis and management of nonalcoholic fatty liver disease: Practice guidance from the american association for the study of liver diseases. Hepatology. 67(1):328-357.

Chalasani N, Younossi Z, Lavine JE, Diehl AM, Brunt EM, Cusi K, Charlton M, Sanyal AJ. 2012. The diagnosis and management

of non−alcoholic fatty liver disease: Practice guideline by the american association for the study of liver diseases, american college of gastroenterology, and the american gastroenterological association. Hepatology. 55(6):2005− 2023.

Chan DC. 2020. Mitochondrial dynamics and its involvement in disease. Annu Rev Pathol. 15:235−259.

Chen H, Detmer SA, Ewald AJ, Griffin EE, Fraser SE, Chan DC. 2003. Mitofusins mfn1 and mfn2 coordinately regulate mitochondrial fusion and are essential for embryonic development. J Cell Biol. 160(2):189−200.

Chen H, Ren S, Clish C, Jain M, Mootha V, McCaffery JM, Chan DC. 2015. Titration of mitochondrial fusion rescues mff−deficient cardiomyopathy. J Cell Biol. 211(4):795−805.

Chih−Hung G, Pei−Chung C. 2012. Mitochondrial free radicals, antioxidants, nutrient substances, and chronic hepatitis c. In: Mohammed Amr E−M, editor. Antioxidant enzyme. Rijeka: IntechOpen. p. Ch. 9.

Choung HW, Lee DS, Lee JH, Shon WJ, Lee JH, Ku Y, Park JC. 2016. Tertiary dentin formation after indirect pulp capping using protein cpne7. J Dent Res. 95(8):906−912.

Cobourne MT, Sharpe PT. 2003. Tooth and jaw: Molecular mechanisms of patterning in the first branchial arch. Arch Oral Biol. 48(1):1−14.

Costiniti V, Bomfim GH, Li Y, Mitaishvili E, Ye ZW, Zhang J, Townsend DM, Giacomello M, Lacruz RS. 2020.

Mitochondrial function in enamel development. Front Physiol. 11:538.

Couve E, Osorio R, Schmachtenberg O. 2013. The amazing odontoblast: Activity, autophagy, and aging. J Dent Res. 92(9):765-772.

Creutz CE. 2012. Copine. In: Choi S, editor. Encyclopedia of signaling molecules. New York, NY: Springer New York. p. 448-453.

Creutz CE, Tomsig JL, Snyder SL, Gautier MC, Skouri F, Beisson J, Cohen J. 1998. The copines, a novel class of c2 domain-containing, calcium-dependent, phospholipid-binding proteins conserved from paramecium to humans. J Biol Chem. 273(3):1393-1402.

Cunha-Cruz J, Wataha JC, Zhou L, Manning W, Trantow M, Bettendorf MM, Heaton LJ, Berg J. 2010. Treating dentin hypersensitivity: Therapeutic choices made by dentists of the northwest precedent network. J Am Dent Assoc. 141(9):1097-1105.

de Brito OM, Scorrano L. 2008. Mitofusin 2 tethers endoplasmic reticulum to mitochondria. Nature. 456(7222):605-610.

Degli Esposti D, Hamelin J, Bosselut N, Saffroy R, Sebagh M, Pommier A, Martel C, Lemoine A. 2012. Mitochondrial roles and cytoprotection in chronic liver injury. Biochem Res Int. 2012:387626.

Docimo R, Montesani L, Maturo P, Costacurta M, Bartolino M, DeVizio W, Zhang YP, Cummins D, Dibart S, Mateo LR. 2009.

Comparing the efficacy in reducing dentin hypersensitivity of a new toothpaste containing 8.0% arginine, calcium carbonate, and 1450 ppm fluoride to a commercial sensitive toothpaste containing 2% potassium ion: An eight-week clinical study in rome, italy. J Clin Dent. 20(1):17-22.

Eckstein M, Vaeth M, Aulestia FJ, Costiniti V, Kassam SN, Bromage TG, Pedersen P, Issekutz T, Idaghdour Y, Moursi AM et al. 2019. Differential regulation of ca(2+) influx by orai channels mediates enamel mineralization. Sci Signal. 12(578).

Eckstein M, Vaeth M, Fornai C, Vinu M, Bromage TG, Nurbaeva MK, Sorge JL, Coelho PG, Idaghdour Y, Feske S et al. 2017. Store-operated ca(2+) entry controls ameloblast cell function and enamel development. JCI Insight. 2(6):e91166.

Ekstedt M, Franzen LE, Mathiesen UL, Thorelius L, Holmqvist M, Bodemar G, Kechagias S. 2006. Long-term follow-up of patients with nafld and elevated liver enzymes. Hepatology. 44(4):865-873.

Ernster L, Schatz G. 1981. Mitochondria: A historical review. J Cell Biol. 91(3 Pt 2):227s-255s.

Favaro Zeola L, Soares PV, Cunha-Cruz J. 2019. Prevalence of dentin hypersensitivity: Systematic review and meta-analysis. J Dent. 81:1-6.

Ferramosca A, Zara V. 2014. Modulation of hepatic steatosis by dietary fatty acids. World J Gastroenterol. 20(7):1746-1755.

Fu Y, Li X, Que K, Wang M, Hu D, Mateo LR, DeVizio W, Zhang YP. 2010. Instant dentin hypersensitivity relief of a new

desensitizing dentifrice containing 8.0% arginine, a high cleaning calcium carbonate system and 1450 ppm fluoride: A 3-day clinical study in chengdu, china. Am J Dent. 23 Spec No A:20A-27A.

Gandolfi MG, Silvia F, H PD, Gasparotto G, Carlo P. 2008. Calcium silicate coating derived from portland cement as treatment for hypersensitive dentine. J Dent. 36(8):565-578.

Gedalia I, Brayer L, Kalter N, Richter M, Stabholz A. 1978. The effect of fluoride and strontium application on dentin: In vivo and in vitro studies. J Periodontol. 49(5):269-272.

Giacomello M, Pyakurel A, Glytsou C, Scorrano L. 2020. The cell biology of mitochondrial membrane dynamics. Nat Rev Mol Cell Biol. 21(4):204-224.

Guo C, Sun L, Chen X, Zhang D. 2013. Oxidative stress, mitochondrial damage and neurodegenerative diseases. Neural Regen Res. 8(21):2003-2014.

Halliwell B, Clement MV, Long LH. 2000. Hydrogen peroxide in the human body. FEBS Lett. 486(1):10-13.

Halliwell B, Gutteridge JMC. 2015. Free radicals in biology and medicine. Oxford University Press. https://doi.org/10.1093/acprof:oso/9780198717478.001.0001.

Hirayama S, Komine C, Takahashi C, Matsui S, Matsushima K. 2013. Effects of calcium carbonate on odontoblast differentiation and calcification ability of human dental pulp cells. Journal of Oral Tissue Engineering. 11(2):123-134.

Holland GR, Narhi MN, Addy M, Gangarosa L, Orchardson R. 1997. Guidelines for the design and conduct of clinical trials on dentine hypersensitivity. J Clin Periodontol. 24(11):808−813.

Horton JD, Goldstein JL, Brown MS. 2002. Srebps: Activators of the complete program of cholesterol and fatty acid synthesis in the liver. J Clin Invest. 109(9):1125−1131.

Hrycay EG, Bandiera SM. 2015. Chapter two − involvement of cytochrome p450 in reactive oxygen species formation and cancer. In: Hardwick JP, editor. Advances in pharmacology. Academic Press. p. 35−84.

Huang M, Hill RG, Rawlinson SC. 2016. Strontium (sr) elicits odontogenic differentiation of human dental pulp stem cells (hdpscs): A therapeutic role for sr in dentine repair? Acta Biomater. 38:201−211.

Ibdah JA, Perlegas P, Zhao Y, Angdisen J, Borgerink H, Shadoan MK, Wagner JD, Matern D, Rinaldo P, Cline JM. 2005. Mice heterozygous for a defect in mitochondrial trifunctional protein develop hepatic steatosis and insulin resistance. Gastroenterology. 128(5):1381−1390.

Imhof T, Rosenblatt K, Pryymachuk G, Weiland D, Noetzel N, Deschner J, Baris OR, Kimoloi S, Koch M, Wiesner RJ et al. 2020. Epithelial loss of mitochondrial oxidative phosphorylation leads to disturbed enamel and impaired dentin matrix formation in postnatal developed mouse incisor. Sci Rep. 10(1):22037.

Ishihara N, Eura Y, Mihara K. 2004. Mitofusin 1 and 2 play distinct

roles in mitochondrial fusion reactions via gtpase activity. J Cell Sci. 117(Pt 26):6535-6546.

Jin Y, Tan Y, Chen L, Liu Y, Ren Z. 2018. Reactive oxygen species induces lipid droplet accumulation in hepg2 cells by increasing perilipin 2 expression. Int J Mol Sci. 19(11).

Karren MA, Coonrod EM, Anderson TK, Shaw JM. 2005. The role of fis1p-mdv1p interactions in mitochondrial fission complex assembly. J Cell Biol. 171(2):291-301.

Kirpich IA, Marsano LS, McClain CJ. 2015. Gut-liver axis, nutrition, and non-alcoholic fatty liver disease. Clin Biochem. 48(13-14):923-930.

Kleinberg I. 2002. Sensistat. A new saliva-based composition for simple and effective treatment of dentinal sensitivity pain. Dent Today. 21(12):42-47.

Knockaert L, Fromenty B, Robin MA. 2011. Mechanisms of mitochondrial targeting of cytochrome p450 2e1: Physiopathological role in liver injury and obesity. FEBS J. 278(22):4252-4260.

Koliaki C, Szendroedi J, Kaul K, Jelenik T, Nowotny P, Jankowiak F, Herder C, Carstensen M, Krausch M, Knoefel WT et al. 2015. Adaptation of hepatic mitochondrial function in humans with non-alcoholic fatty liver is lost in steatohepatitis. Cell Metab. 21(5):739-746.

Koshiba T, Detmer SA, Kaiser JT, Chen H, McCaffery JM, Chan DC. 2004. Structural basis of mitochondrial tethering by mitofusin complexes. Science. 305(5685):858-862.

Krishnasamy Y, Gooz M, Li L, Lemasters JJ, Zhong Z. 2019. Role of mitochondrial depolarization and disrupted mitochondrial homeostasis in non-alcoholic steatohepatitis and fibrosis in mice. Int J Physiol Pathophysiol Pharmacol. 11(5):190-204.

Kumar J, Teoh SL, Das S, Mahakknaukrauh P. 2017. Oxidative stress in oral diseases: Understanding its relation with other systemic diseases. Front Physiol. 8:693.

Kun L. 1976. [biophsical study of dental tissues under the effect of a local strontium application]. SSO Schweiz Monatsschr Zahnheilkd. 86(7):661-676.

Le MH, Yeo YH, Li X, Li J, Zou B, Wu Y, Ye Q, Huang DQ, Zhao C, Zhang J et al. 2021. 2019 global nafld prevalence: A systematic review and meta-analysis. Clin Gastroenterol Hepatol.

Lee JH, Lee DS, Choung HW, Shon WJ, Seo BM, Lee EH, Cho JY, Park JC. 2011. Odontogenic differentiation of human dental pulp stem cells induced by preameloblast-derived factors. Biomaterials. 32(36):9696-9706.

Lee YS, Park YH, Lee DS, Seo YM, Lee JH, Park JH, Choung HW, Park SH, Shon WJ, Park JC. 2020. Tubular dentin regeneration using a cpne7-derived functional peptide. Materials (Basel). 13(20).

Liou YH, Personnaz J, Jacobi D, Knudsen NH, Chalom MM, Starost KA, Nnah IC, Lee CH. 2022. Hepatic fis1 regulates mitochondrial integrated stress response and improves metabolic homeostasis. JCI Insight. 7(4).

Liu C-Y, Tsai C-J, Yasugaki S, Nagata N, Morita M, Isotani A, Yanagisawa M, Hayashi Y. 2021. Copine-7 is required for rem sleep regulation following cage change or water immersion and restraint stress in mice. Neuroscience Research. 165:14-25.

Lopez-Otin C, Blasco MA, Partridge L, Serrano M, Kroemer G. 2013. The hallmarks of aging. Cell. 153(6):1194-1217.

Maharjan BR, McLennan SV, Yee C, Twigg SM, Williams PF. 2021. The effect of a sustained high-fat diet on the metabolism of white and brown adipose tissue and its impact on insulin resistance: A selected time point cross-sectional study. Int J Mol Sci. 22(24).

Mammes O, Aubert R, Betoulle D, Pean F, Herbeth B, Visvikis S, Siest G, Fumeron F. 2001. Lepr gene polymorphisms: Associations with overweight, fat mass and response to diet in women. Eur J Clin Invest. 31(5):398-404.

Mansouri A, Gattolliat CH, Asselah T. 2018. Mitochondrial dysfunction and signaling in chronic liver diseases. Gastroenterology. 155(3):629-647.

Matsuishi YI, Kato H, Masuda K, Yamaza H, Hirofuji Y, Sato H, Wada H, Kiyoshima T, Nonaka K. 2018. Accelerated dentinogenesis by inhibiting the mitochondrial fission factor, dynamin related protein 1. Biochem Biophys Res Commun. 495(2):1655-1660.

Matteoni CA, Younossi ZM, Gramlich T, Boparai N, Liu YC, McCullough AJ. 1999. Nonalcoholic fatty liver disease: A

spectrum of clinical and pathological severity. Gastroenterology. 116(6):1413-1419.

Mears JA, Lackner LL, Fang S, Ingerman E, Nunnari J, Hinshaw JE. 2011. Conformational changes in dnm1 support a contractile mechanism for mitochondrial fission. Nat Struct Mol Biol. 18(1):20-26.

Miglani S, Aggarwal V, Ahuja B. 2010. Dentin hypersensitivity: Recent trends in management. J Conserv Dent. 13(4):218-224.

Mishima H, Sakae T, Kozawa Y. 1995. Scanning electron microscopy and energy dispersive spectroscopy analysis of calciotraumatic lines in rat labial dentin after acute exposure to strontium chloride. Scanning Microsc. 9(3):797-803.

Moore MP, Cunningham RP, Meers GM, Johnson SA, Wheeler AA, Ganga RR, Spencer NM, Pitt JB, Diaz-Arias A, Swi AIA et al. 2022. Compromised hepatic mitochondrial fatty acid oxidation and reduced markers of mitochondrial turnover in human nafld. Hepatology.

Murphy EA, Velazquez KT, Herbert KM. 2015. Influence of high-fat diet on gut microbiota: A driving force for chronic disease risk. Curr Opin Clin Nutr Metab Care. 18(5):515-520.

Murphy MP. 2013. Mitochondrial dysfunction indirectly elevates ros production by the endoplasmic reticulum. Cell Metab. 18(2):145-146.

Musso G, Gambino R, Cassader M, Pagano G. 2011. Meta-analysis: Natural history of non-alcoholic fatty liver disease (nafld)

and diagnostic accuracy of non-invasive tests for liver disease severity. Ann Med. 43(8):617-649.

Nalefski EA, Falke JJ. 1996. The c2 domain calcium-binding motif: Structural and functional diversity. Protein Sci. 5(12):2375-2390.

Nassir F, Ibdah JA. 2014. Role of mitochondria in nonalcoholic fatty liver disease. Int J Mol Sci. 15(5):8713-8742.

Neuschwander-Tetri BA. 2010. Hepatic lipotoxicity and the pathogenesis of nonalcoholic steatohepatitis: The central role of nontriglyceride fatty acid metabolites. Hepatology. 52(2):774-788.

Oh HJ, Choung HW, Lee HK, Park SJ, Lee JH, Lee DS, Seo BM, Park JC. 2015. Cpne7, a preameloblast-derived factor, regulates odontoblastic differentiation of mesenchymal stem cells. Biomaterials. 37:208-217.

Olley RC, Moazzez R, Bartlett D. 2015. Effects of dentifrices on subsurface dentin tubule occlusion: An in situ study. Int J Prosthodont. 28(2):181-187.

Otera H, Wang C, Cleland MM, Setoguchi K, Yokota S, Youle RJ, Mihara K. 2010. Mff is an essential factor for mitochondrial recruitment of drp1 during mitochondrial fission in mammalian cells. J Cell Biol. 191(6):1141-1158.

Park SH, Lee YS, Lee DS, Park JC, Kim R, Shon WJ. 2019. Cpne7 induces biological dentin sealing in a dentin hypersensitivity model. J Dent Res. 98(11):1239-1244.

Park YH, Son C, Seo YM, Lee YS, Har A, Park JC. 2021. Cpne7-

induced autophagy restores the physiological function of mature odontoblasts. Front Cell Dev Biol. 9:655498.

Pashley DH. 1986. Dentin permeability, dentin sensitivity, and treatment through tubule occlusion. J Endod. 12(10):465-474.

Pashley DH, Galloway SE. 1985. The effects of oxalate treatment on the smear layer of ground surfaces of human dentine. Arch Oral Biol. 30(10):731-737.

Pashley DH, Tay FR, Yiu C, Hashimoto M, Breschi L, Carvalho RM, Ito S. 2004. Collagen degradation by host-derived enzymes during aging. J Dent Res. 83(3):216-221.

Pearce NX, Addy M, Newcombe RG. 1994. Dentine hypersensitivity: A clinical trial to compare 2 strontium densensitizing toothpastes with a conventional fluoride toothpaste. J Periodontol. 65(2):113-119.

Peng KY, Watt MJ, Rensen S, Greve JW, Huynh K, Jayawardana KS, Meikle PJ, Meex RCR. 2018. Mitochondrial dysfunction-related lipid changes occur in nonalcoholic fatty liver disease progression. J Lipid Res. 59(10):1977-1986.

Pernas L, Scorrano L. 2016. Mito-morphosis: Mitochondrial fusion, fission, and cristae remodeling as key mediators of cellular function. Annu Rev Physiol. 78:505-531.

Pessayre D, Fromenty B. 2005. Nash: A mitochondrial disease. J Hepatol. 42(6):928-940.

Pessayre D, Mansouri A, Fromenty B. 2002. Nonalcoholic steatosis and steatohepatitis. V. Mitochondrial dysfunction in

steatohepatitis. Am J Physiol Gastrointest Liver Physiol. 282(2):G193-199.

Pessayre D, Mansouri A, Haouzi D, Fromenty B. 1999. Hepatotoxicity due to mitochondrial dysfunction. Cell Biol Toxicol. 15(6):367-373.

Pirola CJ, Gianotti TF, Burgueno AL, Rey-Funes M, Loidl CF, Mallardi P, Martino JS, Castano GO, Sookoian S. 2013. Epigenetic modification of liver mitochondrial DNA is associated with histological severity of nonalcoholic fatty liver disease. Gut. 62(9):1356-1363.

Plumlee GS, Ziegler TL. 2007. 9.07 - the medical geochemistry of dusts, soils, and other earth materials. In: Holland HD, Turekian KK, editors. Treatise on geochemistry. Oxford: Pergamon. p. 1-61.

Rajwani A, Ezzat V, Smith J, Yuldasheva NY, Duncan ER, Gage M, Cubbon RM, Kahn MB, Imrie H, Abbas A et al. 2012. Increasing circulating igfbp1 levels improves insulin sensitivity, promotes nitric oxide production, lowers blood pressure, and protects against atherosclerosis. Diabetes. 61(4):915-924.

Rector RS, Morris EM, Ridenhour S, Meers GM, Hsu FF, Turk J, Ibdah JA. 2013. Selective hepatic insulin resistance in a murine model heterozygous for a mitochondrial trifunctional protein defect. Hepatology. 57(6):2213-2223.

Rector RS, Thyfault JP, Uptergrove GM, Morris EM, Naples SP, Borengasser SJ, Mikus CR, Laye MJ, Laughlin MH, Booth FW

et al. 2010. Mitochondrial dysfunction precedes insulin resistance and hepatic steatosis and contributes to the natural history of non-alcoholic fatty liver disease in an obese rodent model. J Hepatol. 52(5):727-736.

Rizzuto R, Bernardi P, Pozzan T. 2000. Mitochondria as all-round players of the calcium game. J Physiol. 529 Pt 1:37-47.

Rolo AP, Teodoro JS, Palmeira CM. 2012. Role of oxidative stress in the pathogenesis of nonalcoholic steatohepatitis. Free Radic Biol Med. 52(1):59-69.

Ruch JV, Lesot H, Begue-Kirn C. 1995. Odontoblast differentiation. Int J Dev Biol. 39(1):51-68.

Sanyal AJ, Campbell-Sargent C, Mirshahi F, Rizzo WB, Contos MJ, Sterling RK, Luketic VA, Shiffman ML, Clore JN. 2001. Nonalcoholic steatohepatitis: Association of insulin resistance and mitochondrial abnormalities. Gastroenterology. 120(5):1183-1192.

Savino M, d'Apolito M, Centra M, van Beerendonk HM, Cleton-Jansen AM, Whitmore SA, Crawford J, Callen DF, Zelante L, Savoia A. 1999. Characterization of copine vii, a new member of the copine family, and its exclusion as a candidate in sporadic breast cancers with loss of heterozygosity at 16q24.3. Genomics. 61(2):219-226.

Scorrano L. 2009. Opening the doors to cytochrome c: Changes in mitochondrial shape and apoptosis. Int J Biochem Cell Biol. 41(10):1875-1883.

Seo YM, Park SJ, Lee HK, Park JC. 2017. Copine-7 binds to the

cell surface receptor, nucleolin, and regulates ciliogenesis and dspp expression during odontoblast differentiation. Sci Rep. 7(1):11283.

Sharma S, Shetty NJ, Uppoor A. 2012. Evaluation of the clinical efficacy of potassium nitrate desensitizing mouthwash and a toothpaste in the treatment of dentinal hypersensitivity. J Clin Exp Dent. 4(1):e28-33.

Silverman G, Berman E, Hanna CB, Salvato A, Fratarcangelo P, Bartizek RD, Bollmer BW, Campbell SL, Lanzalaco AC, Mackay BJ et al. 1996. Assessing the efficacy of three dentifrices in the treatment of dentinal hypersensitivity. J Am Dent Assoc. 127(2):191-201.

Splieth CH, Tachou A. 2013. Epidemiology of dentin hypersensitivity. Clin Oral Investig. 17 Suppl 1:S3-8.

Tan B, Liu L, Yang Y, Liu Q, Yang L, Meng F. 2019. Low cpne3 expression is associated with risk of acute myocardial infarction: A feasible genetic marker of acute myocardial infarction in patients with stable coronary artery disease. Cardiol J. 26(2):186-193.

Than NN, Newsome PN. 2015. A concise review of non-alcoholic fatty liver disease. Atherosclerosis. 239(1):192-202.

Tielens AG, Rotte C, van Hellemond JJ, Martin W. 2002. Mitochondria as we don't know them. Trends Biochem Sci. 27(11):564-572.

Tomsig JL, Creutz CE. 2002. Copines: A ubiquitous family of ca(2+)-dependent phospholipid-binding proteins. Cell Mol

Life Sci. 59(9):1467-1477.

Twig G, Elorza A, Molina AJ, Mohamed H, Wikstrom JD, Walzer G, Stiles L, Haigh SE, Katz S, Las G et al. 2008. Fission and selective fusion govern mitochondrial segregation and elimination by autophagy. EMBO J. 27(2):433-446.

Twig G, Shirihai OS. 2011. The interplay between mitochondrial dynamics and mitophagy. Antioxid Redox Signal. 14(10):1939-1951.

Venditti P, Di Stefano L, Di Meo S. 2013. Mitochondrial metabolism of reactive oxygen species. Mitochondrion. 13(2):71-82.

Wang KS, Zuo L, Pan Y, Xie C, Luo X. 2015. Genetic variants in the cpne5 gene are associated with alcohol dependence and obesity in caucasian populations. J Psychiatr Res. 71:1-7.

Wang Q, Zou MH. 2018. Measurement of reactive oxygen species (ros) and mitochondrial ros in ampk knockout mice blood vessels. Methods Mol Biol. 1732:507-517.

Weyemi U, Dupuy C. 2012. The emerging role of ros-generating nadph oxidase nox4 in DNA-damage responses. Mutation Research/Reviews in Mutation Research. 751(2):77-81.

Yamada T, Murata D, Adachi Y, Itoh K, Kameoka S, Igarashi A, Kato T, Araki Y, Huganir RL, Dawson TM et al. 2018. Mitochondrial stasis reveals p62-mediated ubiquitination in parkin-independent mitophagy and mitigates nonalcoholic fatty liver disease. Cell Metab. 28(4):588-604 e585.

Yu R, Lendahl U, Nister M, Zhao J. 2020. Regulation of mammalian mitochondrial dynamics: Opportunities and challenges. Front

Endocrinol (Lausanne). 11:374.

Zeichner-David M, Diekwisch T, Fincham A, Lau E, MacDougall M, Moradian-Oldak J, Simmer J, Snead M, Slavkin HC. 1995. Control of ameloblast differentiation. Int J Dev Biol. 39(1):69-92.

Zhang Y-Y, Yang L. 2009. Interactions between human cytochrome p450 enzymes and steroids: Physiological and pharmacological implications. Expert Opinion on Drug Metabolism & Toxicology. 5(6):621-629.

Zhou S, Xie P, Quoibion A, Ambalavanan A, Dionne-Laporte A, Spiegelman D, Bourassa CV, Xiong L, Dion PA, Rouleau GA. 2019. Genetic architecture and adaptations of nunavik inuit. Proc Natl Acad Sci U S A. 116(32):16012-16017.

Zukowski P, Maciejczyk M, Waszkiel D. 2018. Sources of free radicals and oxidative stress in the oral cavity. Arch Oral Biol. 92:8-17.

국문초록

미토콘드리아 기능에 기반하여 CPNE7이
상아모세포 및 간세포에 미치는 영향

황금빛

서울대학교 치의학대학원

치의과학과 세포 및 발생 생물학 전공

(지도교수 박 주 철)

Copine7 (CPNE7)은 칼슘-의존성 인지질결합 단백질의 유비쿼터스한 Copine 패밀리의 멤버로 동물, 식물, 원생생물에서 진화적으로 보존되었다고 알려져 있다. 치아 발생 과정 동안 치아 상피 유래 인자인 CPNE7은 전법랑모세포에서 전상아모세포로 이동하여 상아모세포 분화에 관여한다. 최근에는 CPNE7이 자가포식을 통해서 성숙한 상아모세포의 기능적 재활성화를 유도하고 생리적 상아질 재생에 있어서 중요한 역할을 한다는 것이 확인되었다. CPNE7의 생물학적 역할을 면밀하게 살펴보기 위해, 유전자 표적 시스템을 사용하여 $Cpne7$ 유전자 녹아웃($Cpne7^{-/-}$) 마우스를 제작하였다. $Cpne7^{-/-}$ 마우스의 조직학적 분석에서 손상된 상아모세포와 비정상적인 상아질의 형성이 관찰되었다. CPNE7은 자가포식유도와 관련된 메커니즘 외에도 높은 칼슘 이온 결합력을 가지기 대문에 칼슘 조절에도 관여한다고 알려져

있다. 또한 CPNE7은 산화스트레스를 유발하는 활성산소를 제거할 수 있다는 연구결과가 있다. 칼슘 조절과 활성산소는 모두 미토콘드리아의 기능과 밀접하게 연관이 있으며, 미토콘드리아 기능은 상아모세포의 분화와 상아질형성에 영향을 준다. 그러나 미토콘드리아가 성숙한 상아모세포에 의한 생리학적 상아질 형성에 관여하는 지 여부는 불분명하다.

Cpne7 $^{-/-}$ 마우스의 조직학적 분석에서는 간 지질 축적도 관찰되었다. 최근 연구에서는 지방산 및 지질 대사의 이상이 CPNE7의 유전적 변이와 관련이 있다는 보고가 있었다. 간 지질은 지방 생합성, 지방 조직의 지방 분해, 순환에서의 재흡수를 통한 지방산 유입에 의해 생성된다. 이러한 간 지질은 미토콘드리아에서 지방산의 베타 산화에 의해 제거 될 수 있다. 따라서, 미토콘드리아 기능 장애는 간 지질 항상성에 영향을 미치고 과도한 활성산소 생성을 촉진하여 대사 질환의 근본적인 병인이 될 수 있다. 그러나 간 및 미토콘드리아에서 *Cpne7*의 영향에 대한 연구는 아직 수행된 바가 없다.

따라서, 본 연구에서는 CPNE7이 상아모세포와 간세포의 미토콘드리아에 어떤 영향을 미치는지 알아보고자 하였다. 미토콘드리아의 호흡 측정은 산화스트레스가 유발된 사람치수세포에서 CPNE7 유래 펩타이드를 처리 후 시행되었다. CPNE7-DP는 산화스트레스가 있는 사람치수세포의 최대 미토콘드리아 호흡을 유의하게 증가시켰다. 시험관 내와 생체 내의 상아질 지각과민증 모델에서 CPNE7 유래 펩타이드가 함유된 치약과 시판 중인 지각 과민 완화 치약으로 칫솔질 후 조직학적 분석과 미세누출정도를 평가하였다. 생체 내 상아질 지각과민증 모델 중 CPNE7 유래 펩타이드가 함유된 치약으로 칫솔질 한 실험군에서 유일하게 삼차상아질의 형성을 관찰할 수 있었으며, 미세누출분석에서 대조군에 비하여 유의하게 낮은 수준인

것을 확인하였다.

간세포에서 CPNE7의 기능을 알아보기 위하여 *Cpne7* 유전자 결손 생쥐와 과발현 생쥐에서 고지방식이를 하여 비알코올성 지방간질환 동물 모델을 제작하였고 조직학적 분석, 웨스턴 블랏, 활성산소 수준, 미토콘드리아 기능을 조사함으로써 지질대사이상과 미토콘드리아의 기능장애를 확인하였다. 고지방식이로 유도된 비알코올성지방간 모델의 간세포에서는 *Cpne7* 유전자 결핍이 간세포내에 많은 지방 축적을 야기하였다. 또한 미토콘드리아 역동성의 불균형과 함께 미토콘드리아의 기능이상이 확인됐으며, 이로 인해 높은 활성산소의 수준이 관찰되었다. 이러한 결과는 동물모델에서뿐만 아니라 시험관 내 연구에서도 동일한 결과를 확인할 수 있었다. 이를 통해 *Cpne7* 유전자결핍에 의한 미토콘드리아 기능장애가 간세포에 지방축적을 야기하는 것으로 확인되었다.

따라서, 이 연구는 CPNE7 유래 펩타이드가 산화스트레스하에서 상아모세포의 미토콘드리아 기능을 증가시켜 삼차상아질 형성과 상아질 밀봉효과를 유도할 수 있다는 가능성을 제시한다. 간에서는 *Cpne7* 결핍은 과도한 활성산소 생성과 미토콘드리아 기능 장애를 촉진하여 지질대사이상을 악화시킬 수 있음을 보여주었다. 총괄적으로, 위의 연구들은 CPNE7이 상아모세포 및 간세포의 미토콘드리아 기능에 영향을 주어 상아모세포의 삼차상아질의 형성과 간에서의 지질대사에 각각 중요한 역할을 할 것을 시사한다.